mathematics

MDPI

Article

Advanced Direct Vector Control Method for Optimizing the Operation of a Double-Powered Induction Generator-Based Dual-Rotor Wind Turbine System

Habib Benbouhenni [1] and Nicu Bizon [2,3,4,*]

[1] Department of Electrical & Electronics Engineering, Faculty of Engineering and Architecture, Nisantasi University, Istanbul 34481742, Turkey; habib.benbouenni@nisantasi.edu.tr
[2] Doctoral School, Polytechnic University of Bucharest, 313 Splaiul Independentei, 060042 Bucharest, Romania
[3] Faculty of Electronics, Communication and Computers, University of Pitesti, 110040 Pitesti, Romania
[4] ICSI Energy, National Research and Development Institute for Cryogenic and Isotopic Technologies, 240050 Ramnicu Valcea, Romania
* Correspondence: nicu.bizon@upit.ro

Abstract: The main goal of this paper is to increase the active/reactive power extracted from variable-speed dual-rotor wind power (DRWP) based on doubly-fed induction generators (DFIG) by optimizing its operation using advanced direct vector control. First, the dynamic modeling of different parts of the system is introduced. The DFIG is modeled in the Park reference system. After that, the control techniques are introduced in detail. Direct vector command (DVC) with four-level fuzzy pulse width modulation (FPWM) is used to control the rotor current, thereby controlling the reactive power and active power of the generator. Then, use the neural network design to replace the traditional proportional-integral (PI) controller. Finally, the Matlab/Simulink software is used for simulation to prove the effectiveness of the command strategy using 1.5 MW DRWP. The results show good performance in terms of response time, stability, and precision in following the reference under variable wind speed conditions. In addition, the total harmonic distortion (THD) value of stator current is about 0.13%, being a bit less than other THD values reported in the literature.

Keywords: direct vector command; dual-rotor wind power; four-level fuzzy pulse width modulation; doubly-fed induction generator; proportional-integral controller

Citation: Benbouhenni, H.; Bizon, N. Advanced Direct Vector Control Method for Optimizing the Operation of a Double-Powered Induction Generator-Based Dual-Rotor Wind Turbine System. *Mathematics* **2021**, *9*, 2403. https://doi.org/10.3390/math9192403

Academic Editors: Denis N. Sidorov and Amir Mosavi

Received: 10 August 2021
Accepted: 23 September 2021
Published: 27 September 2021

1. Introduction

Wind turbines (WT) have become the subject of intensive research in recent years, which are focused on optimizing their operation related to reliability, maintenance, costs, and cyber-security issues [1–4]. Two different WTs are usually used: vertical axis WTs (VAWTs) and horizontal axis WTs (HAWT). HAWT has a single rotor turbine (SRWT) and three blades and has been widely used as a traditional kind of WT. On the other hand, a dual-rotor WT (DRWT) is a type of horizontal-axis WT, which consists of two rotors rotating in opposite directions on the same axis [1]. Compared to classic WTs, this type provides higher torque values. In [2], an in-depth critical study between VAWT and HAWT is presented. The research focuses on the challenges facing HAWT, especially in high-energy systems. VAWT offers solutions to some of the direct challenges HAWT faces in terms of reliability, maintenance, and costs, especially in the marine environment. In [3], a new study was introduced to reduce the number of WTs installed in a wind farm based on the Binary Correct Programming Method (BIP). In [4], an integrated fuzzy proportional command is introduced into the dynamic behavior of WT blades together with traditional proportional control to adjust the pitch angle. Today, many installed wind turbines are equipped with doubly-fed induction generators (DFIGs). The DFIG is directly connected to the grid. On the other hand, DFIG is the most important generator for variable speed WTs. Several methods are suggested to command DFIG-based wind power generation

for optimizing its operation, which il be discussed in the next section. The field-oriented control (FOC) method is among the most popular methods used to control DFIG due to its simplicity and ease of implementation. This method is of two types: direct vector control (DVC) and indirect vector control (IVC). The DVC control is simpler compared to the IVC technique. But, the IVC control gives minimum power ripples and harmonic distortion of stator current of DFIG. On the other hand, the main problem with the FOC technique or DVC and IVC technique is that it does not give satisfactory results in the event of a change in the machine's parameters, and this is a negative and undesirable thing. This is due to the use of the proportional-integral (PI) controller and hysteresis comparators. Several research works have been published in this field to improve the performance of the generator, and among the most famous methods that provided better results, we find direct control of torque and direct control of power as the best methods. However, despite the obtained results, the problem of power and current fluctuations remains.

The research topic presented in the present work is the optimal control of a high-power generator integrated into dual-rotor wind power (DRWP). Note that this generator has already been studied in previous works by many authors [5,6].

In this work, a new method is proposed to reduce these ripples as well as significantly improve the performance and efficiency of the DFIG. The method proposed in this paper is mainly based on the modified DVC method as will be presented in this paper. So, in this work, a new method for DVC based on neural networks and a new pulse width modulation (PWM) technique are proposed to optimize the operation of the DFIG-based DRWP system.

To improve the performance of the DVC method (the robustness, no ripples of the active and reactive power, and a minimum value of the total harmonic distortion (THD) of stator current), we propose to use the neural DVC method (NDVC) to integrated the DFIG driver into the DRWP system. New four-level PWM technology based on the fuzzy logic controller is proposed, being easy to use because the structure is simple. This technology reduces the ripples of torque and active power and improves robustness to parameters uncertainty of the DFIG-based DRWP system.

This work puts forward a new DVC control scheme, shows the results of the relevant simulation of the DFIG-based DRWP system, and compares the proposed robust technique with the classic DVC method. The objective of this paper is to apply the designed technique to adjust and command the stator reactive and active power of the DFIG driver provided by the four-level fuzzy PWM technology. The simulation results validate that the NDVC method with the designed four-level FPWM technique has a very robust behavior (almost like the control using a conventional neural network) and it works with low power ripples during the steady-state. So, this proposal presents an optimal DFIG drive command, which is a robust and ripple-free DC technique.

In summary, the novelty and the main contributions of the paper are listed below:

- ✓ A new DVC control scheme is proposed and designed for the DFIG-based DRWP system.
- ✓ The proposed DVC control scheme with fuzzy PWM technique and neural algorithms is a robust strategy compared to classical DVC control with PI controllers and improves the dynamic performances of the DFIG-based DRWP system.
- ✓ The proposed method is simple and therefore easier to implement compared to the traditional technique. In addition, the proposed method reduces the reactive and active power ripples and minimizes the total harmonic distortion value of the stator current of DFIG compared to other reference strategies proposed in the literature.

This work is organized as follows. Section 2 presentation of some work related to this paper. The methodology of research is presented in Section 3 and its subsections. Section 3.1 explains the designed fuzzy PWM technique for a multilevel inverter. The DRWP system is presented in Section 3.2. Section 3.3 explains the traditional DVC method for the DFIG-based DRWP system. The proposed DVC method, which is based on neural algorithms and the four-level fuzzy-PWM technique, has been presented in Section 3.4. Numerical simulation results are presented in Section 4. The conclusion is given in Section 5.

2. Related Work

To identify the research gaps in the field of research addressed in this research study, the main control methods recently proposed in the literature are critically analyzed in this section.

It is worth mentioning that several methods have been proposed to control DFIG to obtain very satisfactory results in terms of current quality, THD value, as well as power ripples. In [7], a finite position set model reference adaptive observer (FPMRAO) method is designed to command doubly-fed induction generators. In [8], a Fractional Proportional Integral (FOPI) controller was proposed to control the Tidal Stream Turbine (TST) based on DFIG. In [9], to improve the characteristic of DFIG, three methods are combined. These methods are heart exchange optimization (TEO), fuzzy controller, and second-order sliding mode control (SOSMC). In [10], a new technique based on amplitude control was designed to control WTs based on doubly-fed induction machines. The performance of DFIG-based wind turbines is improved through the direct power control (DPC) of the SOSMC controller [11]. In [12], the behavior of a fully developed DFIG-wind turbine system model was studied using MATLAB software® under defective situations. More precisely, short-circuit faults in both the rotor terminals and back-to-back inverter are checked at typical wind speeds. It has been proposed to combine two methods, which are different in principle, to minimize torque ripples and reactive power fluctuations of the DFIG-based dual-rotor WT (DRWT) [13]. The first method is based on the super twisting algorithm (STA) and the second is based on the synergetic control theory. The proposed technique is more robust and it is easier to adjust the tuning parameters compared to the classical method. In [14], the terminal sliding mode controller (TSMC) reduced the harmonics and ripples of the DFIG current compared to the traditional SMC method. In [15], a new strategy was designed based on a new fractional-order command strategy to minimize active power and current ripples of DFIG. The simulated results show that the current ripples are lower than when using the fractional-order control strategy. In [16], a new strategy is designed for the DFIG control. This strategy is based on the backstepping control and Lyapunov theory. This designed strategy is a simple algorithm that gives better results than the classic method. In [17], a new DPC method was designed based on the fuzzy-genetic algorithm (FGA) to reduce torque and active power ripples of DFIG. The designed strategy improves transient response speed and overall precision as well as significantly minimizing stator current ripples under non-ideal grid conditions. In [18], a robust nonlinear method for wind turbines based on DFIG is proposed. The main idea in [18] is to use backstepping control to decouple DFIG stator reactive and active power for better performance. In [19], a new robust technology based on state feedback linearization control technology is designed to control doubly-fed induction machines. The power ripples are reduced by using the proposed technique. The simulation results show the characteristics of the proposed control technique. In [20], an improved DPC control was proposed to control DFIG. The operation of the improved DPC strategy is based on the principle of stator voltage-oriented command (VOC), in which the voltage is aligned with the quadrature axis of the rotating reference frame. In [21], a subsynchronous damping control (SDC) technique was designed to suppressed the subsynchronous resonance (SSR) of the doubly-fed generator. In [22], a coordinated stator reactive and active power control strategy based on model predictive control (MPC) was designed for DFIG-based WTs with distributed energy storage systems (ESS). The design method is simple and the stator current harmonics are among the smallest reported in the literature. In [23], a new adaptive SOSMC-DPC strategy for DFIG driven by wind turbines is proposed. Comparative numerical simulations are performed under the three DPC technologies on a 2 MW DFIG under unbalanced and balanced grid voltages. Adaptive gain SOSMC-DPC realizes reactive and active power regulation under the two-phase fixed reference frame of unbalanced and balanced grid voltage. In [24], DC voltage regulation has been proposed to control doubly-fed motors. This design technique is a simple control solution, but it does not reduce the ripples of reactive and active power. In [25], to reduce power ripples, the author proposed a robust

nonlinear super-twisting fractional-order TSMC (STFOTSMC)for the rotor-side and grid-side converters of 2 MW DFIG. In [26], the author proposed a novel adaptive high-order SMC to suppressed the subsynchronous control interaction of the WT based on the series-compensated DFIG. Proposed DFIG voltage modulation DPC uses extended power theory under unbalanced grid voltage conditions. Four different methods were compared with each other to determine which technique is superior to other methods in reducing the active power ripple ofDFIG [27]. The results show that, compared with partial feedback linearization, the adaptive STA method can reduce the active power ripple. In [28], a traditional stator flux-based FOC technique based on a full-order adaptive observer is proposed to control the doubly-fed induction machines. The proposed technique is simple and easy to implement. The proposed technique improves the characteristics of generator-based wind power. A non-linear control technique for grid-connected current source converter (CSC) is proposed in [29]. The nonlinear control technology of active power and reactive power of a doubly-fed generator is realized by feedback linearization. A fuzzy-SOSMC control for doubly-fed induction machines is proposed in [30]. This proposed strategy is a robust technique that improves the response time of the active and reactive power compared to the traditional technique. On the other hand, the fuzzy-SOSMC control reduced the active and reactive power ripples. In [31], posteriori multi-objective optimization (MOO) is applied to adjust the parameters of SOSMC control technology, which commands the grid-side converter (GSC) of DFIG in such a way that it is not affected by unbalanced and harmonic distortions of the grid voltage. In [32], direct torque control (DTC) is applied to DFIG driven by WTS connected to the grid. The method is based on the regulation of torque and rotor flux, which are indirect estimates using voltage and current. Comparing these estimated variables with the reference values using the traditional hysteresis comparator will result in digital control signals. A new DPC control technique based on DFIG and grid-connected WTS is proposed [33]. The designed DPC method uses nonlinear SMC technology to directly calculate the required rotor control voltage to eliminate the instantaneous error of stator reactive and active power, without the need for non-linear control based on SMC technology. In [34], the nonlinear control based on the SMC technique has been proposed to minimize the ripple of both torque and active power of the doubly-fed motor. Fuzzy fractional order robust command has been designed to control WT conversion systems based on doubly-fed machines [35], being experimentally tested using a processor-in-the-loop (PIL). In [36], the author proposed the DPC method for DFIG by using a neural algorithm with a multilayer perceptron structure (MPS). This design technique generates quadrature and direct-axis rotor voltage signals based on the voltage and the stator current measured by the Hall sensors. The input variables of the design method are reactive power, rotor speed, and active power reference values, and their respective errors. The designed technology is easy to implement and can minimize the ripples of active power, current, and torque of the doubly-fed motor. Other methods have been proposed with the same objective in the following scientific works [37–41]. In [42], the FOC technique is the most commonly used method in the DFIG command. This technique uses linear controller proportional-integral (PI) to control the DFIG converter. Two different types of traditional FOC strategies are used to command and regulate the reactive and active power of doubly-fed generators. The first method is direct vector control (DVC) and the second method is indirect vector control (IVC). In [43], a DVC technique based on neural space vector modulation (NSVM) technology is proposed. However, the proposed technique gives minimum ripples in current, torque, reactive power compared to traditional DVC with the PWM technique. On the other hand, the proposed strategy improves the response dynamics of the DFIG-based wind power. In [44], a DVC strategy based on the fuzzy SVM strategy was proposed to reduce the ripples of current, flux, and torque of DFIG. An indirect vector control (IVC) is proposed to minimize the current, active power, and torque ripples of the DFIG using the two-level fuzzy space vector PWM technique [45]. The IVC strategy based on the neuro-fuzzy method with the traditional SVM technique is proposed to reduce the current and torque ripples of the

induction generator [46]. This proposed method is simple, robust, and gives minimum power ripple compared to the classical IVC command. In [47], the authors presented a nonlinear controller based on the sliding mode control to maximize the extracted energy of the DFIG controlled by the IVC technique. The proposed technique is more robust compared to the traditional technique. In [48], the authors presented an IVC method based on the hysteresis rotor current controller. The experimental results showed the superiority of the designed IVC strategy. The traditional IVC control scheme for DFIG-based WT systems is a simple algorithm, which has a fast dynamic response in comparison with other well-developed technique approaches, such as the traditional DVC method. The simplicity of this strategy is given by the use of PI regulators for the reactive and active power. However, the controller is linear, and the regulator has a non-constant switching frequency.

There is a multitude of strategies proposed to improve the efficiency of the generator and the quality of the electricity generated, some of which are presented in Appendix A. The main features of these methods and the proposed method were summarized in Table A1 for correct comparison of the reported performance and the identification of research gaps.

The following section will present the modeling and design of the command-and-control blocks integrated into the proposed control technique.

3. Material and Method

To understand the research work performed in this paper, the design, testing, and validation stages of the NDVC-FPWM control method are shown in Figure 1 and presented in the next subsections.

Also, the details of the design stages are presented in the appendices.

3.1. Fuzzy PWM Technique

In the field of energy electronics, traditional PWM technology is the core of AC motor control and has been proven effective in driving modern semiconductor power devices. Most energy electronic circuits are controlled by various forms of traditional PWM signals. The PWM strategy is an effective command strategy, usually used as a command strategy for generating analog signals from digital devices such as microcontrollers. On the other hand, there are three traditional kinds of PWM strategies: leading-edge modulation, trailing-edge modulation, and pulse center two edge modulation/phase correction PWM.

The PWM signal is normally obtained, as in Figure 2. To get a PWM signal, we need two signals of different shapes and frequencies. The first signal is a sinusoidal signal and the second is, for example, a sawtooth signal. The latter has a frequency greater than the sinusoidal signal. In addition, we need a comparator to compare these two signs. The comparator compares the two signals and generates a PWM signal as its output waveform. If the value of the sawtooth signal is greater than the PWM signal, the PWM output signal is in the "high" state, otherwise, it is in the "low" state. Therefore, the value of the input signal amplitude determines the output of the comparator, which defines the pulse width generated at the output [49]. Traditional PWM technology has many advantages compared with other modulation strategies used in AC machines. For example, the PWM technology is simple, provides accuracy and fast response time. It provides a high input power factor, low initial cost, and is easy to implement. The PWM strategy can help the motor to produce maximum torque even at low speeds. However, the PWM technology has the following disadvantages. Due to the high PWM frequency, the switching loss is quite high. It can cause radio frequency interference. This strategy provides a high THD value for the current [49]. In [50], the author proposed to apply PWM technology and neural algorithms to wind turbines based on DFIG. In [51], a three-level PWM technology based on fuzzy logic controllers is proposed. The designed modulation strategy can achieve a fast transient response, while the THD of the output voltage is very low during steady-state operation.

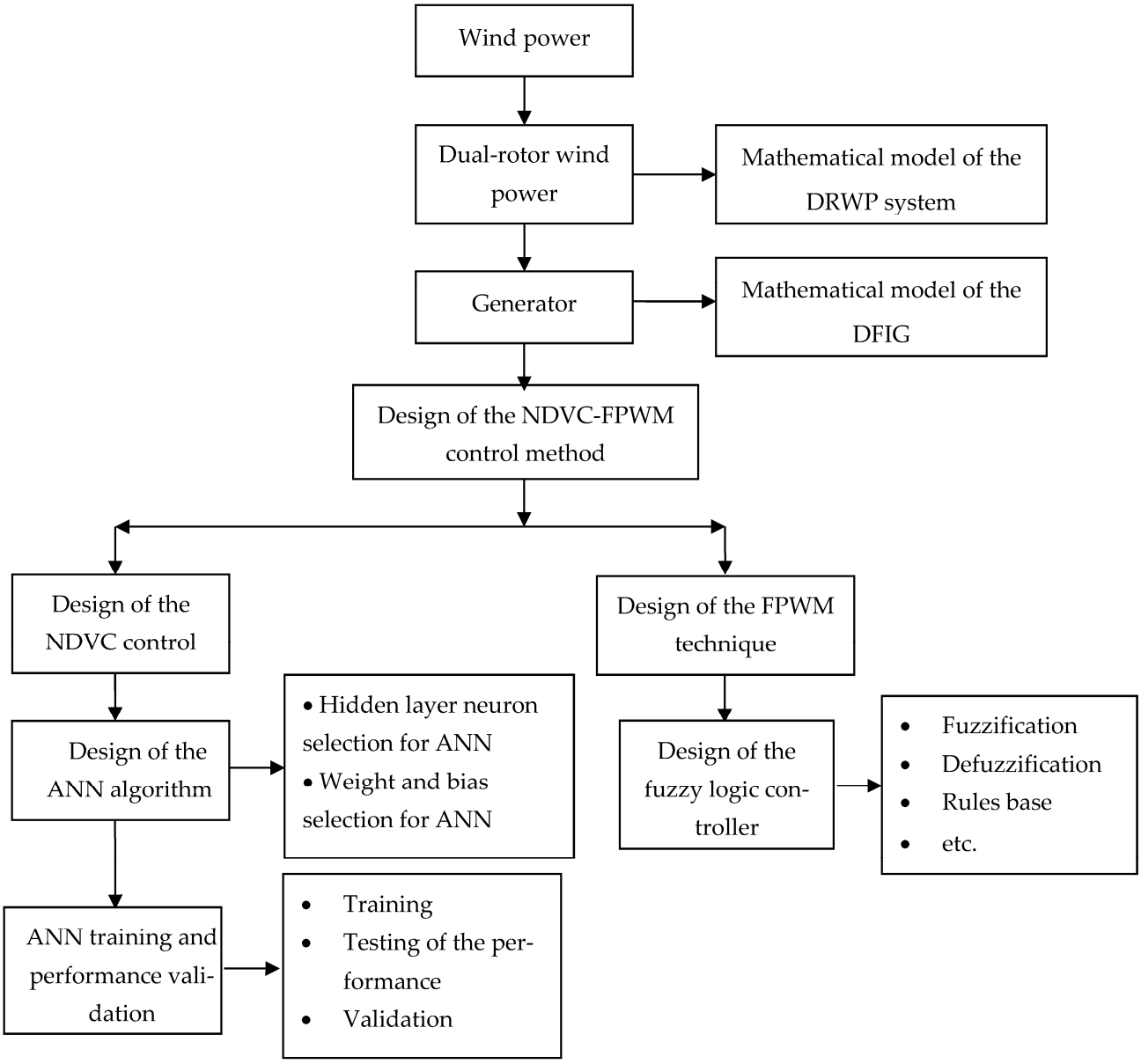

Figure 1. Diagram of research steps followed in this paper.

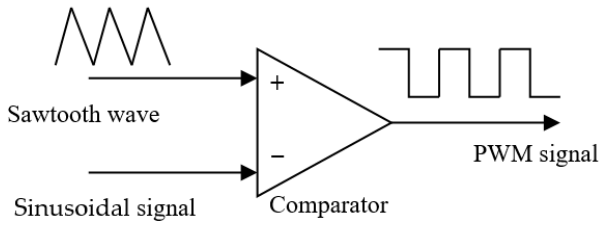

Figure 2. Generation of PWM signal.

In this work, we use the four-level PWM method to command the converter of the DFIG-based DRWT systems. Figure 3 shows the structure of the four-level PWM method. In a four-level PWM strategy, three-phase voltages are compared with three sawtooth waves.Three comparators are used In a four-level PWM strategy to generates a PWM signal. The structure of the hysteresis comparators of the four-level PWM technique is shown in Figure 4. Comparing with the space vector modulation technique, the four-level PWM strategy is a simple algorithm, gives fewer current ripples, easy to implement,

fast response time, and is less dependent on DFIG-DRWP parameters. But the four-level strategy generates a variable-frequency control signal.

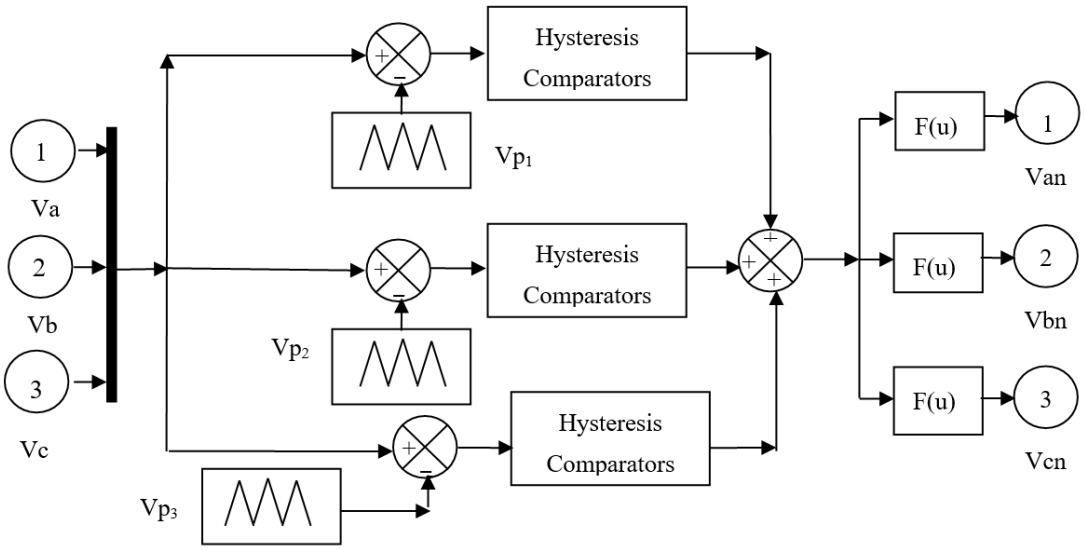

Figure 3. Conventional four-level PWM strategy.

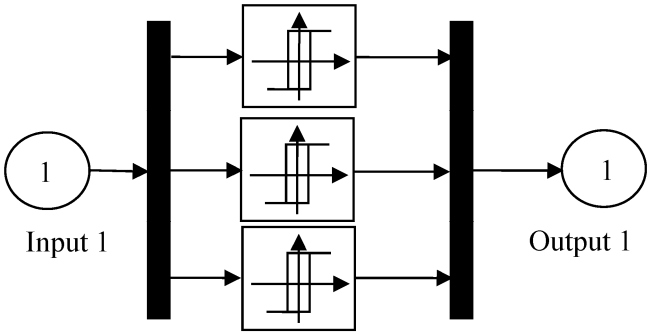

Figure 4. Traditional hysteresis controllers.

To improve the effectiveness of the DFIG in the context of DRWT production, we propose a hybrid modulation technique the combines fuzzy logic and PWM strategy. Figure 5 shows the basic structure of a 4-level fuzzy PWM technique. This strategy is a modification of the conventional four-level PWM strategy, where the hysteresis comparator has been replaced by a fuzzy logic controller (FLC). This designed modulation technique is a simple scheme, robust, and reduced the THD of the current compared to SVM and conventional4-level PWM strategy. In addition, the structure of the fuzzy hysteresis controllers of the 4-level PWM technique is shown in Figure 6.

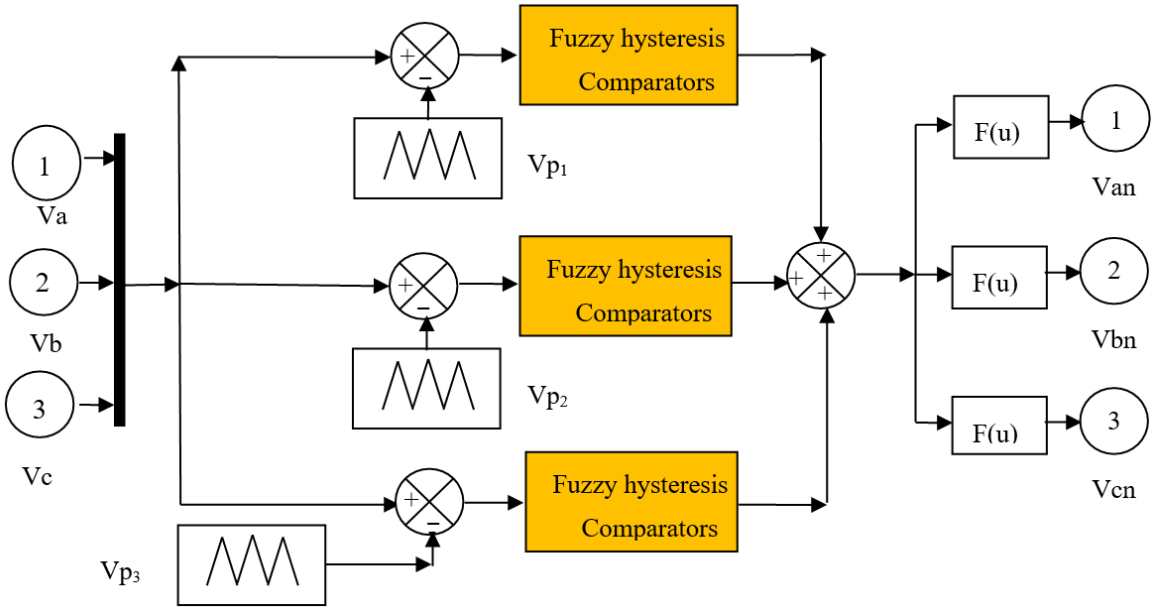

Figure 5. Schematic diagram of the four-level fuzzy PWM strategy.

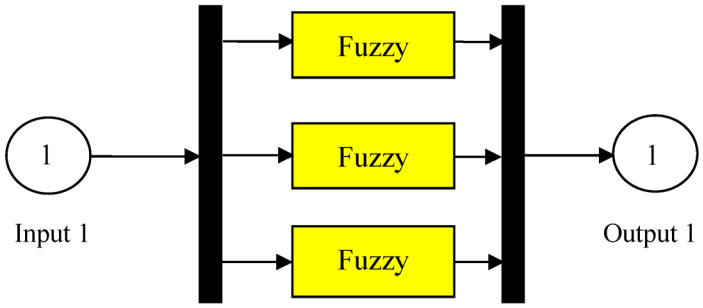

Figure 6. Schematic diagram of the FLC hysteresis comparators.

The FLC methods are widely used for system identification, control, pattern recognition problems, and many other applications developed in academia and applied in industry. However, the fuzzy logic theory was first designed by Zadeh [52] in 1965. This technique is a method based on observation and engineering experience. This technique is widely used in AC motor drive commands [53–55].

The membership degree of an element to the set is defined by the following Equation (1):

$$A = (x, \mu_A(x)) | \forall\, x \in X \tag{1}$$

where $\mu_A : X \to [01]$.

In this condition, $\mu_A(x)$ represents the MF degree of the element $x \in X$ to set A. In this paper, we will use the following notation: $A(x) = \mu_A(x)$ for all $x \in X$. The design of the fuzzy logic controller has been detailed in Appendix B.

3.2. DRWP Model

The DRWP system is a wind turbine for solving both problems that are based on a single rotor WT (SRWT). The DRWP uses two wind turbines rotating in opposite directions on the same axis. However, the SRWT system is the most common WT used the generates electrical energy. The mathematical model of the DRWP is different from the SRWT system. The DRWP system has been proposed as new wind power, as shown in Figure 7. The DRWP system gives more power coefficient and aerodynamic torque compared to the SRWT system. The DRWP system design is composed of two wind turbines, the main turbine and the auxiliary turbine [56]. The control of the DRWP system is difficult

compared to the SRWT system. The total aerodynamic power of the DRWP system is the auxiliary turbine power (P_A) add to the main turbine power (P_M) as shown by the following equation:

$$P_{DRWT} = P_T = P_M + P_A \tag{2}$$

where:

P_M: Main turbine power.
P_A: Auxiliary turbine power.
P_T: Total aerodynamic power.

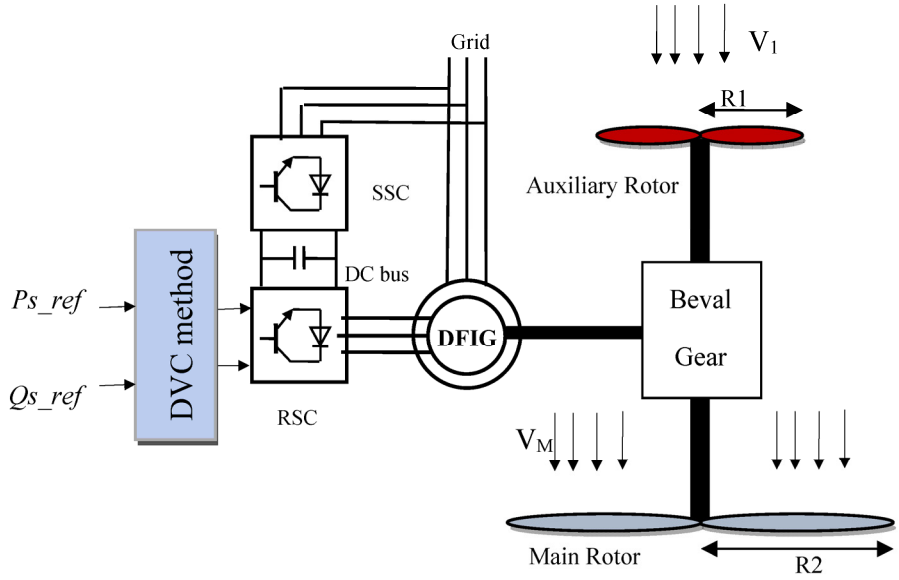

Figure 7. Block diagram of DRWP with a DFIG.

The total torque of the DRWT system is given:

$$T_T = T_M + T_A \tag{3}$$

where:

T_M: Main turbine torque.
T_A: Auxiliary turbine torque.
T_T: Total aerodynamic torque.

Equation (4) represents the aerodynamic torque of the auxiliary turbine [57].

$$T_A = \frac{C_p}{2\lambda_A^3}\rho \cdot \pi \cdot R_A^5 \cdot w_A^2 \tag{4}$$

Equation (5) represents the aerodynamic torque of the main turbine.

$$T_M = \frac{C_p}{2\lambda_M^3}\rho \cdot \pi \cdot R_M^5 \cdot w_M^2 \tag{5}$$

where λ_A and λ_M are the tip speed ratio of the main and auxiliary turbines, ρ is the air density, R_M and R_A are the blade radius of the auxiliary and main turbines, and w_M and w_A are the mechanical speed of the main and auxiliary turbines.

The tip speed can be given by Equations (6) and (7) for the auxiliary and main turbines, respectively.

$$\lambda_A = \frac{w_A \cdot R_A}{V_1} \tag{6}$$

$$\lambda_M = \frac{w_M \cdot R_M}{V_M} \tag{7}$$

where V_M is the speed of the unified wind on the main turbine and V_1 is the wind speed on an auxiliary turbine.

Wind speed is used at the level of the main and auxiliary turbines to calculate the tip speed ratio.

Equation (8) is used to calculate the wind speed at any point between the main and auxiliary turbines.

$$V_x = V_w \cdot \left(1 - \frac{1 - \sqrt{(1 - C_T)}}{2}\left(1 + \frac{2x}{\sqrt{1 + 4x^2}}\right)\right) \tag{8}$$

where V_x is the velocity of the disturbed wind between rotors at point x (x is the non-dimensional distance from the auxiliary rotor disk), and C_T is the thrust coefficient ($C_T = 0.9$). In our work, we take a value of x as 15 m, which denotes the distance between the rotors [57].

The power coefficient is given by the following equations:

$$C_p(\beta, \lambda) = 0.517\left(\frac{116}{\lambda_i} - 0.4\beta - 5\right)e^{\frac{-21}{\lambda_i}} + 0.0068\lambda \tag{9}$$

$$\frac{1}{\lambda_i} = \frac{1}{\lambda + 0.08 \cdot \beta} - \frac{0.035}{\beta^3 + 1} \tag{10}$$

where β is pitch angle.

The DFIG is the most popular variable-speed generator for wind power applications due to its lower cost, control flexibility, and superior performance. The mathematical form of the generator is illustrated by the following equations:

$$\begin{cases} V_{dr} = R_r I_{dr} - W_r \Psi_{qr} + \frac{d}{dt}\Psi_{dr} \\ V_{qr} = R_r I_{qr} + W_r \Psi_{dr} + \frac{d}{dt}\Psi_{qr} \\ V_{qs} = R_s I_{qs} + W_s \Psi_{ds} + \frac{d}{dt}\Psi_{qs} \\ V_{ds} = R_s I_{ds} - W_s \Psi_{qs} + \frac{d}{dt}\Psi_{sd} \end{cases} ; \begin{cases} \Psi_{dr} = L_r I_{dr} + M I_{ds} \\ \Psi_{qr} = M I_{qs} + L_r I_{qr} \\ \Psi_{qs} = M I_{qr} + L_s I_{qs} \\ \Psi_{ds} = L_s I_{ds} + M I_{dr} \end{cases} \tag{11}$$

Equation (12) represents the mechanical equation of the generator.

$$T_e - T_r = J\frac{d\Omega}{dt} + f\Omega \tag{12}$$

Equation (13) represents the torque equation of the generator.

$$T_e = 1.5\, p\frac{M}{L_s}\left(-\Psi_{sd} I_{rq} + \Psi_{sq} I_{rd}\right) \tag{13}$$

where f is the viscous friction coefficient, p is the number of pole pairs, T_r is the load torque, Ω is the mechanical rotor speed, and J is the moment of inertia.

The active and reactive power can be calculated from Equation (14):

$$\begin{cases} P_s = 1.5\left(V_{qs} \cdot I_{qs} + I_{ds} \cdot V_{ds}\right) \\ Q_s = 1.5\left(-I_{qs} \cdot V_{ds} + V_{qs} \cdot I_{ds}\right) \end{cases} \tag{14}$$

3.3. DVC Method

DVC or direct vector control using traditional PI is the most used strategy for DFIG-based wind turbines. In this method, two PI regulators are used to controlling the reactive and active powers [42]. However, this method is easy to implement and simple algorithm compared to indirect vector control. This strategy is detailed in [43,44]. Simplicity is one of the most important features of this method.

The principle of operation is to orient the stator flux along the axis of the rotating frame.

$$\psi_{ds} = 0 \text{ and} \psi_{qs} = \psi_s \tag{15}$$

Equation (16) represents the stator voltage equation of the generator.

$$\begin{cases} V_{qs} = V_s = w_s \cdot \psi_s \\ V_{ds} = 0 \end{cases} \tag{16}$$

A stator current can be written by Equation (17).

$$\begin{cases} I_{qs} = -\frac{M}{L_s} I_{qr} \\ I_{ds} = -\frac{M}{L_s} I_{dr} + \frac{\psi_s}{L_s} \end{cases} \tag{17}$$

A stator reactive/active power can be written by Equation (18) [41].

$$\begin{cases} Q_s = -1.5\left(\frac{\omega_s \psi_s M}{L_s} I_{dr} - \frac{\omega_s {\psi_s}^2}{L_s}\right) \\ P_s = -1.5\frac{\omega_s \psi_s M}{L_s} I_{qr} \end{cases} \tag{18}$$

A torque can be written by Equation (19).

$$T_{em} = -1.5\ I_{qr}.\ \psi_{ds}.\ p.\frac{M}{L_s} \tag{19}$$

The expressions for both V_{qr} and V_{dr} are given by Equation (20) [41–44]:

$$\begin{cases} V_{qr} = R_{dr} \cdot I_{qr} + \left(L_r - \frac{M^2}{L_s}\right) p \cdot I_{qr} - g \cdot w_s \left(L_r - \frac{M^2}{L_s}\right) I_{dr} + g \frac{M \cdot V_s}{L_s} \\ V_{dr} = R_{dr} \cdot I_{dr} + \left(L_r - \frac{M^2}{L_s}\right) p \cdot I_{dr} - g \cdot w_s \left(L_r - \frac{M^2}{L_s}\right) I_{qr} \end{cases} \tag{20}$$

Hence, V_{qr} and V_{dr} can be written as:

$$\begin{cases} V_{qr} = R_{dr} \cdot I_{qr} - g \cdot w_s \left(L_r - \frac{M^2}{L_s}\right) I_{dr} + g \frac{M \cdot V_s}{L_s} \\ V_{dr} = R_{dr} \cdot I_{dr} - g \cdot w_s \left(L_r - \frac{M^2}{L_s}\right) I_{qr} \end{cases} \tag{21}$$

A rotor current can be written by Equation (22).

$$\begin{cases} I_{qr} = \left(V_{qr} - g \cdot w_s \left(L_r - \frac{M^2}{L_s}\right) I_{qr} - g \frac{M \cdot V_s}{L_s}\right) \frac{1}{R_r + \left(L_r - \frac{M^2}{L_s}\right) p} \\ I_{dr} = \left((V_{dr} - g \cdot w_s \left(L_r - \frac{M^2}{L_s}\right) I_{qr}\right) \frac{1}{R_r + \left(L_r - \frac{M^2}{L_s}\right) p} \end{cases} \tag{22}$$

Starting from Equations (15) to (22), we can give a figure by which we explain the principle of operation of the DVC method. Figure 8 shows the structure of the traditional DVC technique. The objective of this method is to obtain the reference rotor voltages (*Vrd** and *Vrq**) from the active and reactive power errors by using two PI controllers.

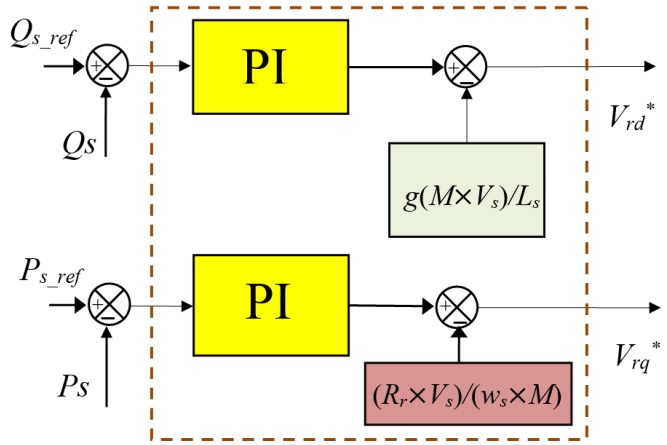

Figure 8. Structure of the traditional DVC method.

Traditionally, DVC control is a simple technique used to control the active power of the DFIG-based wind power. This strategy is easy to implement compared to IVC control. The traditional DVC with PI controllers, which are designed to command the reactive and active powers of the DFIG-based DRWP, is shown in Figure 9. As is known, the purpose of the DVC-PI control is to obtain a direct and quadrature rotor voltages (*Vrd** and *Vrq**) in order to control the inverter. The Park transform is used to obtain the three-phase voltage (*Va*, *Vb*, *Vc*) from *Vrd** and *Vrq**. Despite its simplicity and ease of implementation, this method gives greater fluctuations to current, active power, and torque. On the one hand, the dynamic response is long compared to the IVC method and other techniques.

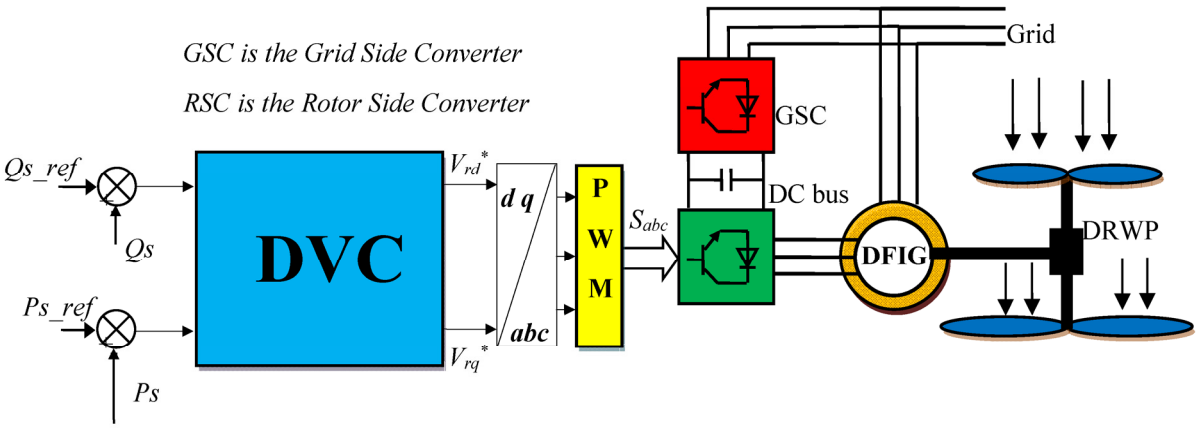

Figure 9. DVC method of three-phase DFIG-based DRWP system.

To improve the performance of the traditional DVC control of the DFIG using the PWM technique, neural networks can be used in the place of the PI regulator, as well as the use of the FPWM technique in the place of the traditional PWM strategy. In this way, we get a more solid strategy and advantages that lead to the better. This proposed method will be explained in Section 3.4 of this paper.

3.4. Neural DVC Method with FPWM Technique

The neural DVC method (NDVC) with the five-level FPWM technique has been designed as a novel design for the improvement of current output, reactive and active power ripples, as shown in Figure 10. The objective of this proposed method is to obtain high quality *Vrd** and *Vrq** from active and reactive power errors. In this method, the direct and quadrature rotor voltages (*Vrd** and *Vrq**) are regulated by the neural networks (see Figure 11). From the observation of Figure 11, we find that the values of both *Vrd** and *Vrq** are related to neural networks, in contrast to the classical method, with the aim of obtaining

*Vrd** and *Vrq** of high quality, thus reducing generator maintenance and extending the life of the inverter.

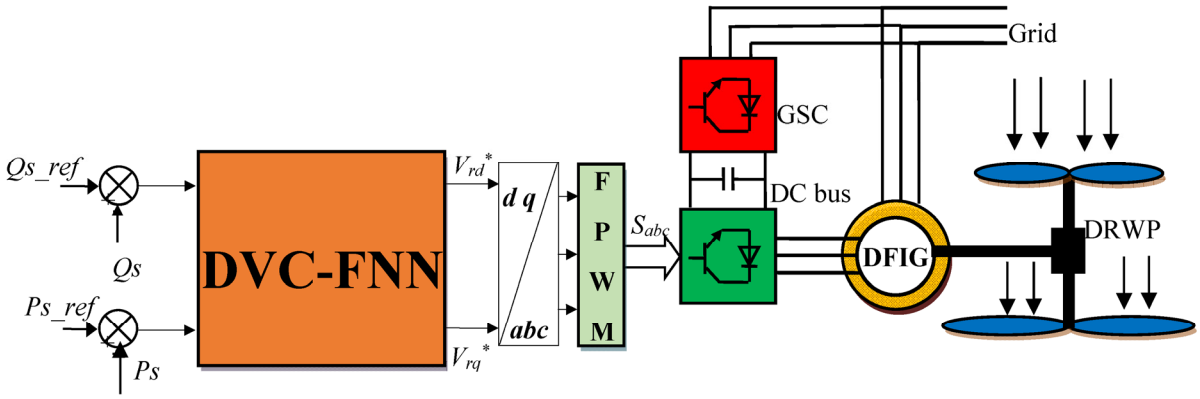

Figure 10. DVC-FNN method of the DFIG-DRWP.

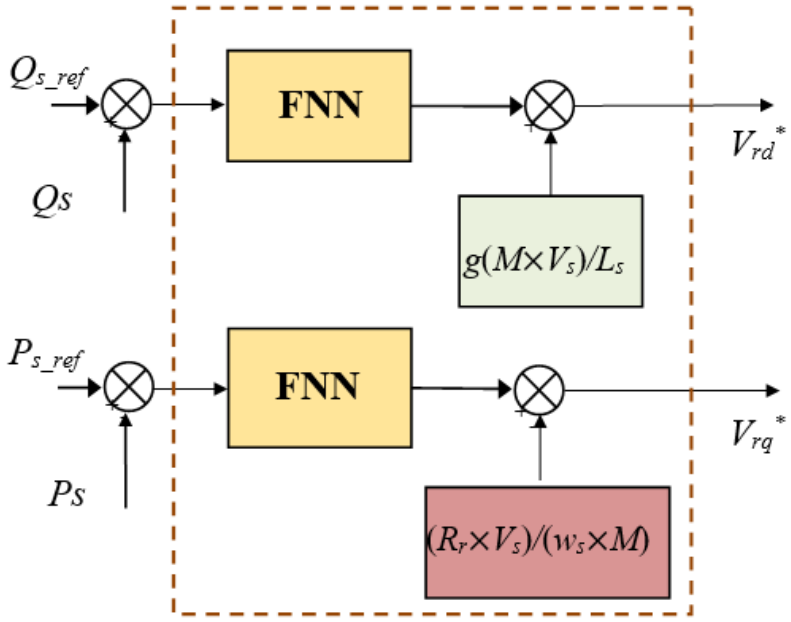

Figure 11. Structure of the DVC-FNN method.

This method was proposed to improve the quality of the current and power generated by the generator-based DRWP system. The proposed DVC technique is simple to control and easy to implement. Durability is one of the main things we get through this proposed DVC method and that's because of the use of neural networks and fuzzy logic controller. Also, by this proposed DVC method or intelligent DVC, the dynamic response of the generator is greatly improved. This proposed method is a change in the form of the classic method, where neural networks were used instead of the conventional PI controller and FPWM was used instead of PWM.

So, two neural controllers are being applied: a neural controller for the reactive power and another neural controller for the active power. The error for reactive and active powers controllers can be specified as follows:

$$\begin{cases} S_r = Q_{s_{ref}} - Q_s \\ S_a = P_{s_{ref}} - P_s \end{cases} \quad (23)$$

Compared with the classical DVC method, the NDVC method ensures diverse advantages such as the reduction of active power ripples, torque ripples, reactive power ripples, constant switching frequency operation, and a robust command scheme. Moreover, it keeps a simple command algorithm, with minor changes to the basic algorithm of the DVC method.

In this work, feedforward neural networks (FNNs) are used [58,59].

The schematic diagram of the FNN controller based on the Levenberg–Marquardt algorithm is shown in Figure 12. This controller is more robust compared to other algorithms.

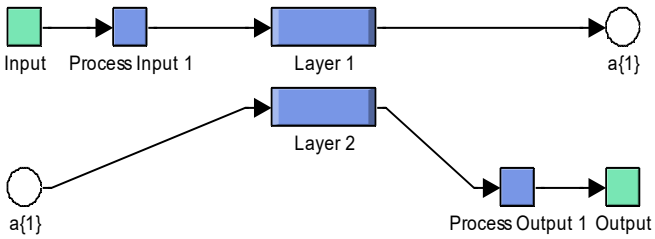

Figure 12. FNN controller.

On the other hand, the schematic diagram of layer 1, layer 2, and a hidden layer is shown in Figures 13–15, respectively.

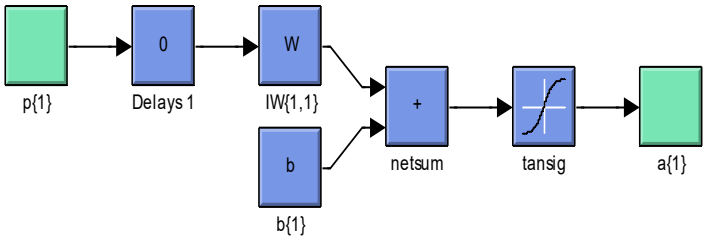

Figure 13. Layer 1.

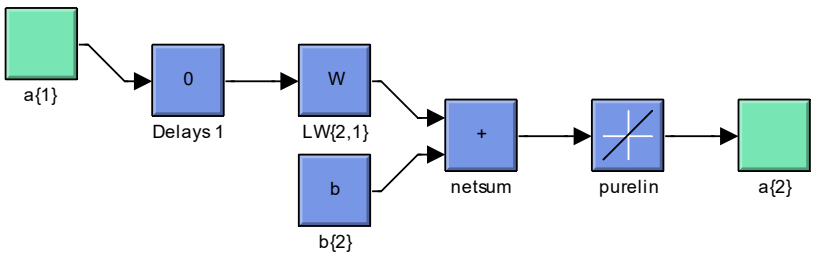

Figure 14. Layer 2.

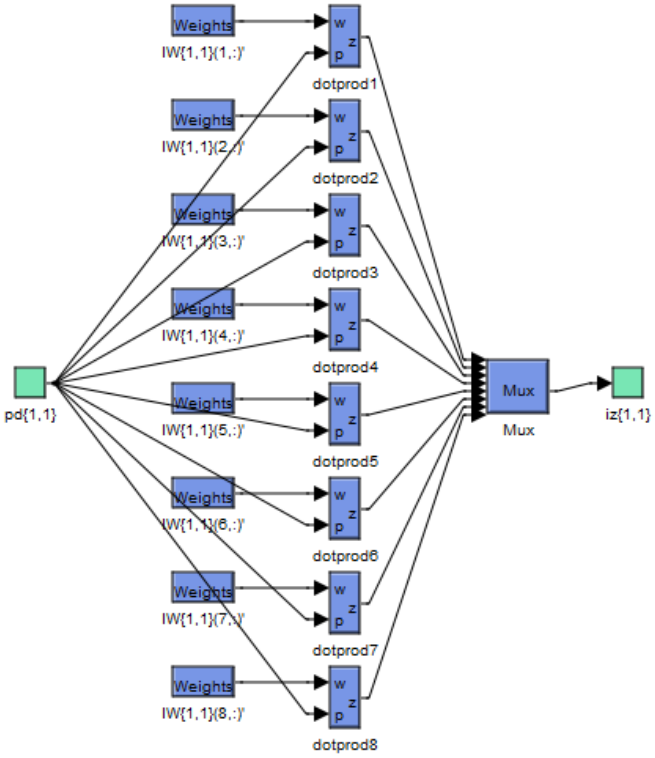

Figure 15. Schematic diagram of the hidden Layer.

The design of the FNN controller has been detailed in Appendix C.

4. Results

The simulation results of the NDVC control with the four-level FPWM technique (NDVC-FPWM) of the DFIG-based DRWT system are compared with the classical DVC technique.

The parameters of the generator are as follows: 380/696 V, R_s = 0.012 Ω, P_{sn} = 1.5 MW, L_r = 0.0136 H, L_m = 0.0135 H, p=2, 50 Hz, J = 1000 kg·m^2, R_r = 0.021 Ω, L_s = 0.0137 H, and f_r = 0.0024 N·m/s.

The simulation signals of the measured and reference active power (Ps) of the DFIG-based DRWT system are shown in Figures 16–23 to compare the effectiveness of the NDVC-FPWM command scheme with the effectiveness of the classical DVC command. The Ps tracks almost perfectly their reference value $P_{s\text{-}ref}$ (see Figure 16). In addition, the amplitudes of the ripples of the stator Ps are smaller and occur in a shorter period in comparison with the ripples obtained for the NDVC-FPWM command scheme (see Figure 21).

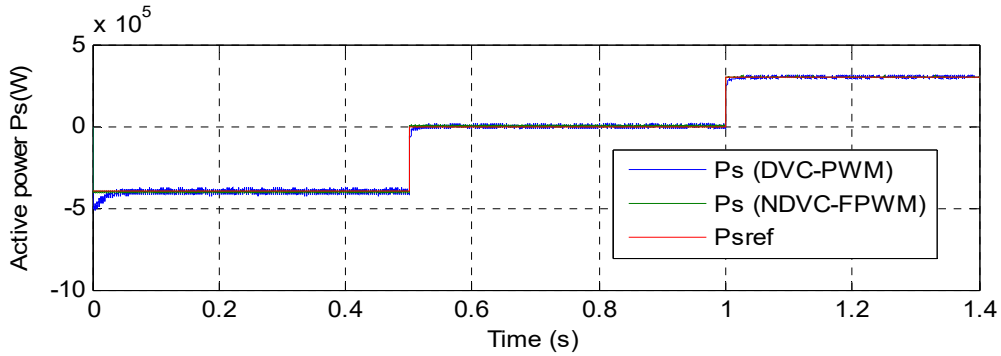

Figure 16. Active power.

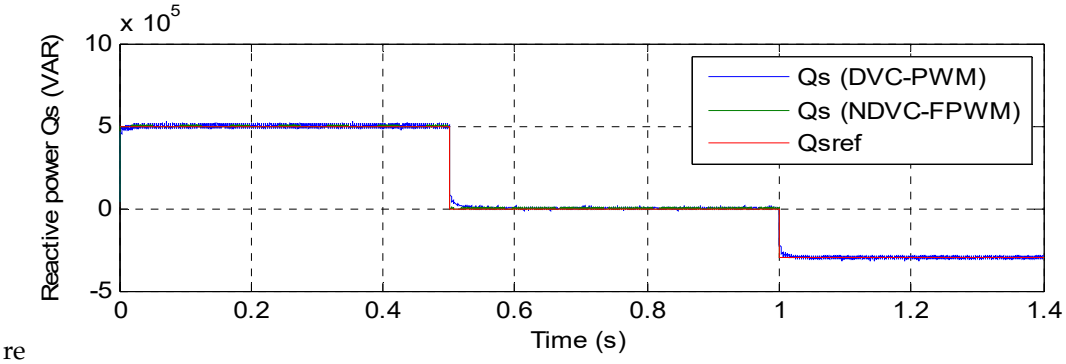

re

Figure 17. Reactive power.

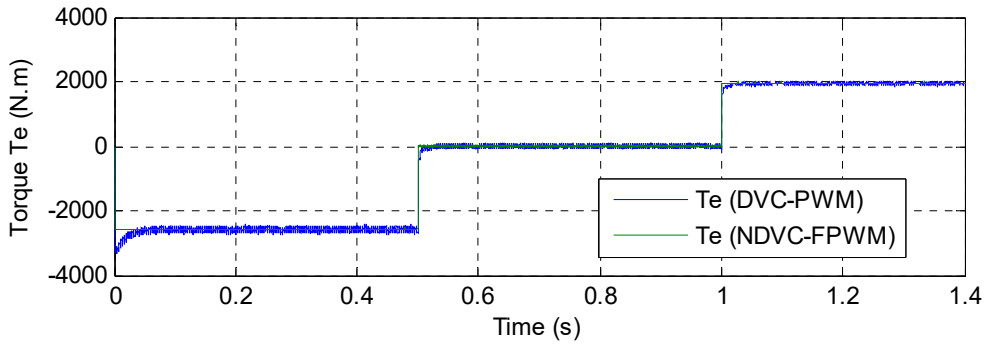

Figure 18. Torque.

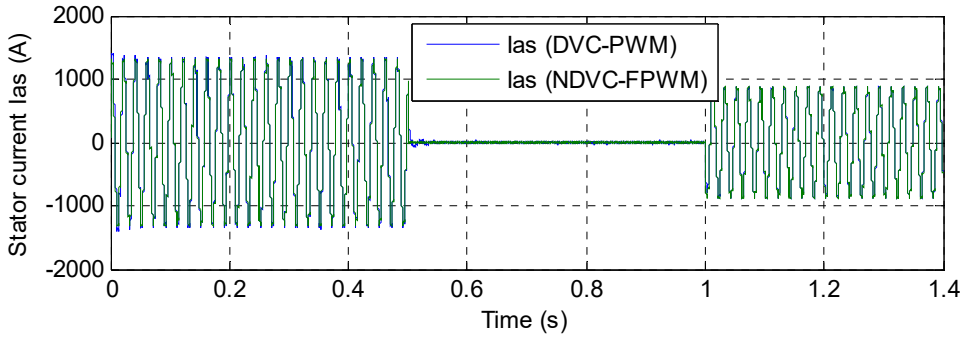

Figure 19. Stator current.

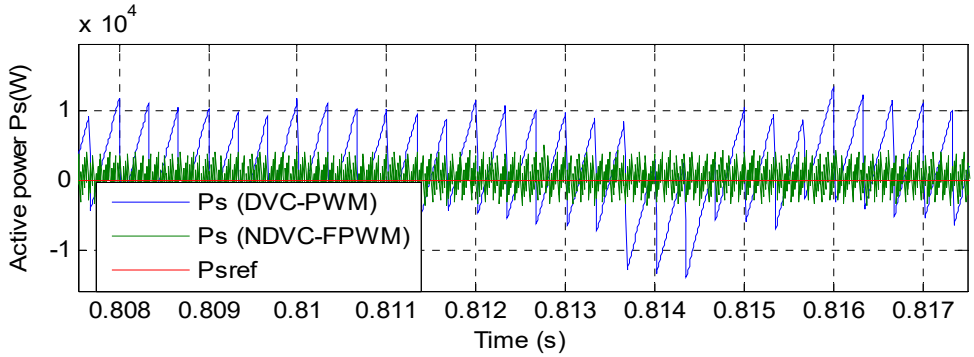

Figure 20. Zoom in the *Ps*.

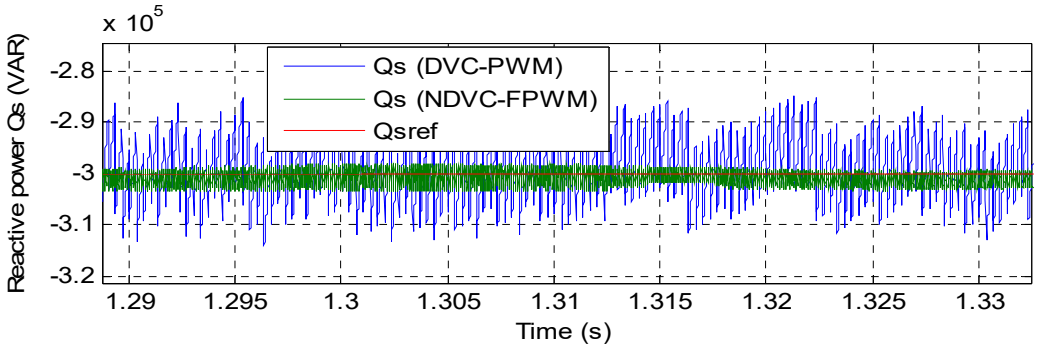

Figure 21. Zoom in the *Qs*.

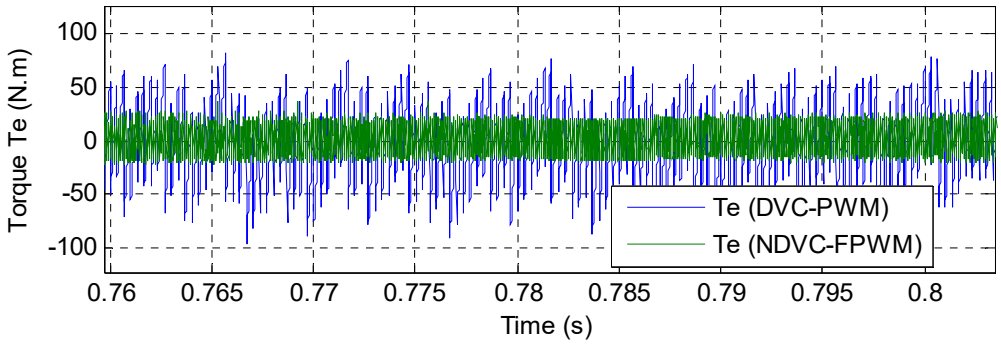

Figure 22. Zoom in the torque.

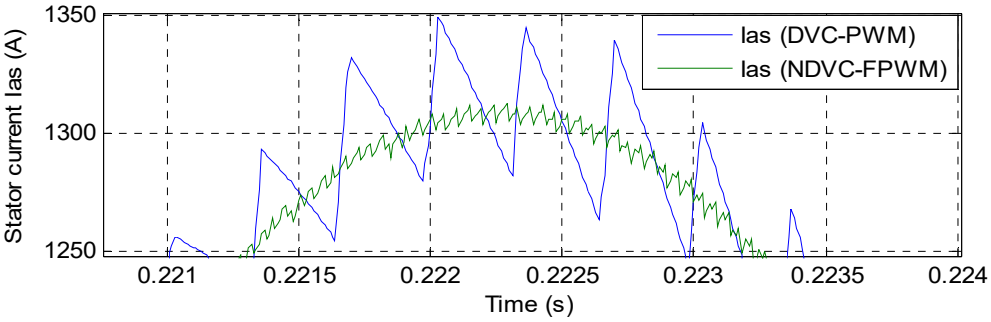

Figure 23. Zoom in the *Ias*.

For the classical DVC and NDVC-FPWM command schemes, the reactive power (*Qs*) tracks almost perfectly their reference value (see Figure 17). Moreover, the NDVC-FPWM command technique minimized the *Qs* ripple compared to the traditional DVC command (see Figure 17).

The waveforms of the torque of both control schemes are shown in Figure 18. It can be said by comparing this figure with Figure 16 that the value of the torque is related to the value of the active power. In addition, the proposed command scheme reduced the torque compared to the classical DVC command (see Figure 22).

The current obtained from the proposed methods in this work is shown in Figure 19. It can be said by observing Figure 23 and comparing it with Figure 21 that the resulting electric current is related to both the system and the reference value of the active power. This can be confirmed by the same form of current and effective power, where the greater the effective power, the greater the current, and vice versa. In addition, the classical DVC command gives more ripple in current compared to the NDVC-FPWM command scheme (See Figure 23). However, the NDVC-FPWM command scheme reduced more the response time of the torque, reactive power, current and active power compared to the classical DVC command (See Table 1).

Table 1. Comparative analysis of response time.

	Response Time		
	Torque	**Active Power**	**Reactive Power**
DVC-PWM	0.036 s	0.036 s	0.014 s
NDVC-FPWM	1.78 ms	1.78 ms	8.5 ms

On the other hand, Figures 24 and 25 show the THD value of the classical DVC with the PWM technique and NDVC-FPWM command scheme respectively. From mentioned Figures, it can be said that the THD value is minimized for the NDVC-FPWM strategy (0.13%) when compared to the traditional DVC command (1.65%). The proposed method reduced the THD value by about 92.12%.

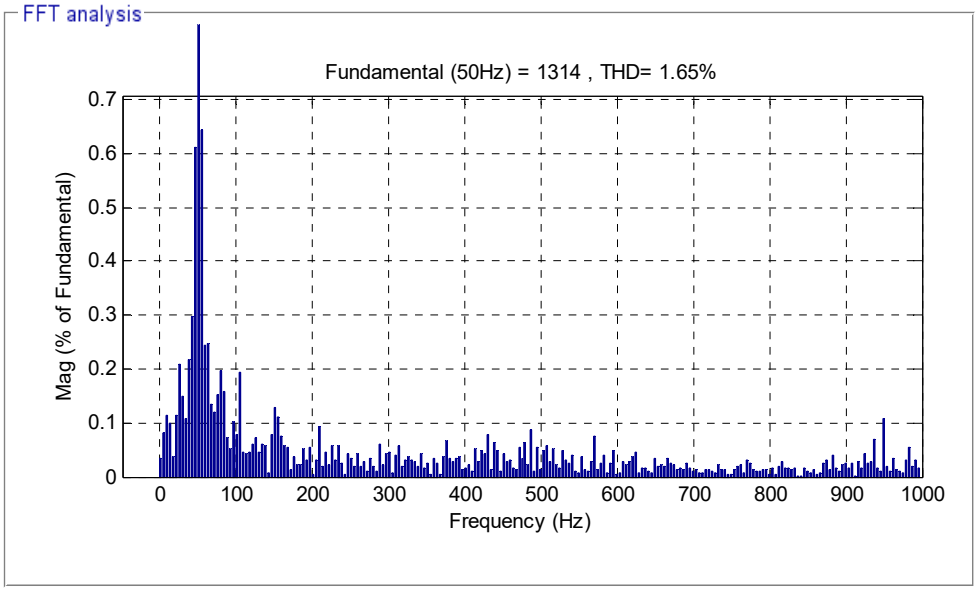

Figure 24. THD (DVC).

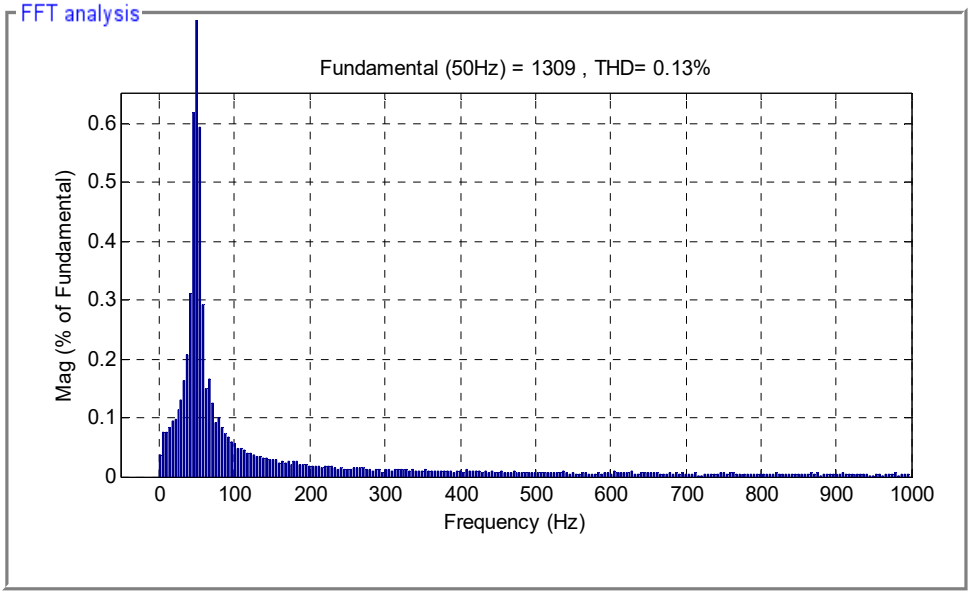

Figure 25. THD (NDVC-FPWM).

The proposed method can be compared with the classical method from several aspects, for example, the dynamic response, simplicity, the value of reactive power ripples, etc. Table 2 shows a comparative study between the proposed methods, according to the results obtained from the numerical simulation. The proposed NDVC-FPWM technique is more robust than the traditional DVC using PI controllers except for the dynamic response, rise time, overshoot, settling time which is faster in the proposed technique than the traditional technique. On the other hand, the proposed method provided better results in terms of reactive power fluctuations, reactive and active power tracking, the quality of the produced current. But the proposed technique is complicated in calculations compared to DVC control.

Table 2. Comparative results were obtained from the NDVC-FPWM with the DVC control.

Criteria	Control Techniques	
	DVC	**NDVC-FPWM**
Reactive and active power tracking	Well	Excellent
Dynamic response (s)	Medium	Fast
Reduce active and reactive power ripples	Acceptable	Excellent
THD (%)	1.65	0.13
Settling time (ms)	High	Medium
Active power ripple (W)	Around 2000	Around 800
Sensitivity to parameter change	High	Medium
Overshoot (%)	Remarkable ≈ 12%	Neglected
Simplicity of converter and filter design	Simple	Simple
Torque: ripple (N.m)	Around 170	Around 50
Rise Time (s)	High	Medium
Reactive power ripple (VAR)	Around 1700	Around 980
Simplicity of calculations	Simple	Rather complicated
Stator current: ripple (A)	Around 100	Around 15
Quality of stator current	Acceptable	Excellent
Improvement of transient performance	Good	Excellent

The response time obtained in this work can be compared with two different control techniques studied in [60]. We find that the NDVC-FPWM control provided a very small time compared to DPC and neuro-second-order sliding mode control. The values are shown in Table 3. The proposed method reduced the response time to active power by approximately 64.4% and 90.11% compared with NSOSMC and DPC, respectively. As for the reactive potential, the ratio was about 5.55% and 50%, compared with NSOSMC and DPC, respectively.

Table 3. Comparison between the proposed method and some methods in terms of response time.

		Response Time		
		Torque	**Reactive Power**	**Active Power**
Proposed technique: NDVC-FPWM		1.78 ms	8.5 ms	1.78 ms
Ref. [60]	Neuro-second order sliding mode control (NSOSMC)	5 ms	9 ms	5 ms
	Direct power control (DPC)	18 ms	17 ms	18 ms

In the end, we study a comparison between the designed strategy and several published works in terms of the percentage of the THD of electric current. The results are recorded in Table 4. Through this table, we note that the proposed method gave much lower percentages of the THD than some of the published methods. So, it can be said that the designed strategy in this work gives a sinusoidal current that has good characteristics in terms of ripples and THD value compared to the rest of the controls, and this is what makes the life of the devices longer and reduces the cost of maintenance.

Table 4. Summary table of results obtained compared to other methods.

Reference	Strategy	THD (%)
Ref. [61]	DTC control	2.57
Ref. [47]	FOC control	3.7
Ref. [55]	Classical DTC method	6.70
	Fuzzy DTC method	2.40
Ref. [62]	DPC with PI controllers	0.43
Ref. [63]	12 sectors DPC(12-DPC) control	0.40
Ref. [64]	Fuzzy SMC method	1.15
Ref. [65]	SOSMC method	3.13
Ref. [66]	DPC control with STA controller	1.66
Ref. [67]	DVC control with synergetic sliding mode controller	0.50
Ref. [68]	Integral sliding mode control (ISMC)	9.71
	Multi-resonant-based sliding mode controller (MRSMC)	3.14
Ref. [69]	DPC with terminal synergetic controller	0.25
Ref. [70]	Two-level DTC control	8.75
	Three-level DTC control	1.57
Ref. [71]	Intelligent super twisting sliding mode controller	0.52
Proposed strategy	Traditional DVC control	1.65
	NDVC-FPWM control	0.13

5. Conclusions

This work presents the simulation results of the high-performance DVC method for a DFIG-based DRWT system. In this paper, the converter of the DFIG is controlled by the five-level FPWM technique. The proposed control methods have been validated by Matlab simulation and the results obtained show a good tracking of the predefined references regardless of the reference powers changing.

The current injected into the grid has a low THD value, being equal to 0.13%. The proposed method presents lower active power, stator current, reactive power, and torque ripples of the DFIG-based DRWT system.

To summarize, the main findings of this research are as follows:

- A new four-level FPWM technique was presented and confirmed with numerical simulation.
- A new DVC control scheme based on neural network and four-level FPWM technique was presented and confirmed with numerical simulation.
- Minimizes the reactive power, stator current, electromagnetic torque, and active power ripples.
- A robust control scheme was proposed.
- Reduce the harmonic distortion of stator current.

In a future paper, to improve the quality of the reactive and active powers, the DFIG will be controlled using another combination of intelligent algorithms, such as genetic algorithm and PSO algorithm used for DFIG in [72].

Author Contributions: Conceptualization, H.B.; methodology, H.B.; software, H.B.; validation, N.B.; investigation, H.B.; resources, H.B. and N.B.; data curation, N.B.; writing—original draft preparation, H.B.; supervision, N.B.; Funding acquisition: N.B.; Visualization: N.B.; writing—review and editing: N.B.; project administration, N.B.; Formal analysis: N.B. and H.B. All authors have read and agreed to the published version of the manuscript.

Funding: There is no funding available for this.

Institutional Review Board Statement: Not applicable.

Informed Consent Statement: Not applicable.

Data Availability Statement: Not applicable.

Conflicts of Interest: The authors declare no conflict of interest.

Abbreviations

List of Symbols:

ϕ_r, ϕ_r*	Actual and reference rotor flux
T_e, T_e*	Actual and reference torques
ω_n, ω_r	Nominal and rotor speeds
θr	Rotor flux angle
p	Generator pole pairs
λ	Tip speed ration
Vm	*Wind speed*
Pn	Nominal Power
V_s, I_s	Vectors of the stator voltage and current
$Vr_{a,b,c}$, $Ir_{a,b,c}$	Rotor voltage and current in *abc* frame
$V_{\alpha,\beta}$, $I_{\alpha,\beta}$	Voltage and current in $\alpha\beta$ frame
R_s, R_r	Stator and rotor resistances
$\phi_{\alpha s}$, $\phi_{\beta s}$	Stator flux components in $\alpha\beta$ frame
Ω	Ohm (unit)
Ki, Kp	Integral and proportional gains
Lr, Ls, Lm	Rotor, stator, and mutual inductances
wb	Weber (unit)
Hz	Hertz (unit)
MW	Migawatt (Unit)
mH	Millihenry (unit)
N.m	Newton-meter (Unit)

List of Acronyms:

DVC	Direct vector control
PI	Proportional integral
FLC	fuzzy logic controller
FNN	Feedforward neural networks
DPC	Direct power control
SMC	Sliding mode control
IVC	Indirect vector control
VAWT	Vertical axis wind turbine
HAWT	Horizontal axis wind turbine
THD	Total harmonic distortion
PWM	Pulse width modulation

FOC	Field-oriented control
DRWT	Dual-rotor wind turbine
FSMC	Fuzzy sliding mode control
TSMC	Terminal sliding mode controller
SVM	Space vector modulation
IP	Integral-proportional
DFIG	doubly-fed induction generator
FPWM	Fuzzy Pulse width modulation
DRWP	Dual-rotor wind power
NDVC	Neural direct vector control
MRSMC	Multi-resonant-based sliding mode controller
ISMC	Integral sliding mode controller.

Appendix A

Table A1. A comparative study of different techniques based on DFIG-Wind turbine.

References	Study Nature	Control	Controller	Type of Generator	Complexity	Current Oscillations	Reference Tracking	Dynamic Responses
Ref. [7]	Simulation	FOC	PI	DFIG	Low	High	++	+
Ref. [8]	Simulation	FOC	FOPI	DFIG	High	Low	+++	++
Ref. [9]	Simulation	Nonlinear control	Fuzzy SOSMC	DFIG	High	Neglected	+++	+++
Ref. [10]	Simulation	Amplitude control	PI	DFIG	Low	Low	++	++
Ref. [11]	Simulation	DPC	SOSMC	DFIG	High	Neglected	+++	++++
Ref. [12]	Simulation	FOC	PI	DFIG	Low	High	++	+
Ref. [13]	Simulation	DPC	Synergetic STA	DFIG	Medium	Low	+++	++++
Ref. [14]	Simulation	Nonlinear control	TSMC	DFIG	High	Neglected	+++	+++
Ref. [15]	Simulation	Fractional-order command	FOPI	DFIG	Medium	Low	+++	++
Ref. [16]	Simulation	Nonlinear control	Backstepping control	DFIG	High	Neglected	+++	+++
Ref. [17]	Simulation	DPC	FGA	DFIG	Medium	Low	++	+++
Ref. [18]	Simulation	DPC	Backstepping control	DFIG	High	Neglected	+++	++++
Ref. [19]	Simulation	Nonlinear control	Feedback linearization control	DFIG	High	Neglected	+++	++
Ref. [20]	Simulation	DPC	VOC	DFIG	Medium	Low	++	+++
Ref. [21]	Simulation	SDC	SDC	DFIG	Medium	Low	++	+++
Ref. [22]	Simulation	DPC	MPC	DFIG	Medium	Low	+++	+++
Ref. [23]	Simulation	DPC	SOSMC	DFIG	High	Low	++++	++++
Ref. [24]	Simulation	DPC	DC voltage regulation	DFIG	Medium	Low	+++	++
Ref. [25]	Simulation	FOC	STFOTSMC	DFIG	High	Low	+++	+++
Ref. [26]	Simulation	DPC	Adaptive High SMC	DFIG	High	Low	+++	++++
Ref. [27]	Simulation	DPC	Extended power theory	DFIG	Medium	High	+++	++
Ref. [28]	Simulation	FOC	Full-order adaptive observer	DFIG	High	Low	++	++

Table A1. *Cont.*

References	Study Nature	Control	Controller	Type of Generator	Complexity	Current Oscillations	Reference Tracking	Dynamic Responses
Ref. [29]	Experimental	Nonlinear control	Feedback linearization	DFIG	High	Low	+++	+++
Ref. [30]	Simulation	Nonlinear control	Fuzzy SOSMC	DFIM	High	Neglected	++++	++++
Ref. [31]	Simulation	SOSMC	MOO	DFIG	Medium	Low	++	+++
Ref. [32]	Simulation	DTC	Hysteresis comparator	DFIG	Medium	High	++	++
Ref. [33]	Simulation	DPC	SMC	DFIG	Medium	Neglected	++++	+++
Ref. [34]	Simulation	Nonlinear control	SMC	DFIG	High	Neglected	++	+++
Ref. [35]	Experimental	Nonlinear control	Fuzzy fractional order robust command	DFIG	High	Neglected	+++	++++
Ref. [36]	Simulation	DPC	MPS	DFIG	Medium	Low	++	+++
Ref. [37]	Simulation	DPC	Neural controller	DFIG	Medium	Low	++++	+++
Ref. [38]	Simulation	FOC	PI	DFIG	Low	High	++	+
Ref. [39]	Simulation	DTC	Resonant current control	DFIG	Medium	High	+++	++
Ref. [40]	Simulation	DTC	PI	DFIG	Low	Low	+++	++
Ref. [41]	Simulation	FOC	PI	DFIG	Low	High	++	+
Ref. [42]	Simulation	FOC	Neuro-fuzzy	DFIG	Medium	Low	++	++
Ref. [43]	Simulation	DVC	Fuzzy SMC	DFIG	Medium	Neglected	++++	+++
Ref. [44]	Simulation	FOC	Neural SOSMC	DFIG	High	Low	++	+++
Ref. [45]	Simulation	DVC	PI	DFIG	Low	High	++	+
Ref. [46]	Experimental	IVC	PI	DFIG	Low	High	++	+
Ref. [47]	Simulation	DPC	Neuro-fuzzy	DFIG	Medium	Low	+++	+++
Ref. [48]	Experimental	IVC	Hysteresis rotor current controller	DFIG	Medium	Low	++	++

Appendix B. Design of the Fuzzy Logic Controller

The fuzzy inference process usually includes four parts: fuzzification, fuzzy rules base, inference method, and defuzzification, as shown in Figure A1. To accomplish fuzzy logic, some steps must be followed which are necessary. These steps are a design of the fuzzy logic system (FLS), fuzzifications, applying the rule-based system, and defuzzification. These steps are necessary to accomplish fuzzy logic, and they depend in particular on experience and observation.

Among the most popular types of FLSs are Tsukamoto, Sugeno, Mamdani, and Larsen. However, Mamdani is the most widely used type, especially in the field of controlling electrical machines, and this is due to the characteristics that make it the most widely used than the rest of the types. On the other hand, the Mamdani fuzzy inference system can be divided into many modules, namely, fuzzifier, fuzzy knowledge-base, inference engine, and de-fuzzifier. The combination of the rules base and the database is referred to as the knowledge base. A rules base has IF-THEN rules, and the database contains fuzzy sets. The fuzzifier uses the MFs stored in the fuzzy knowledge base to convert the crisp input into a linguistic variable [54].

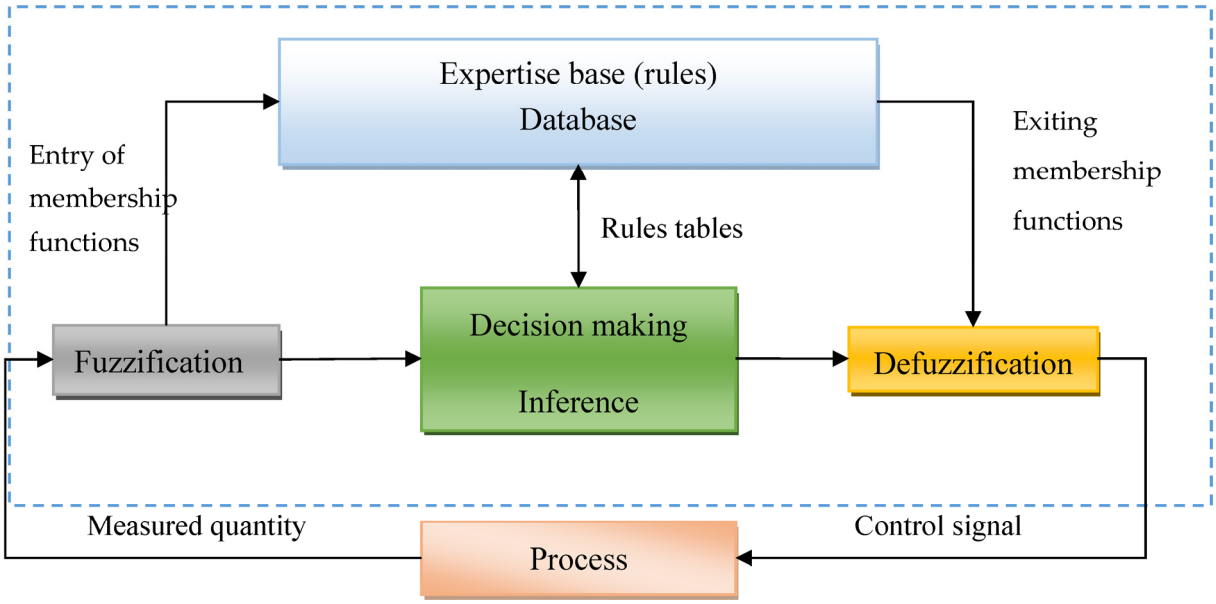

Figure A1. Structure of a fuzzy regulator.

The fuzzy logic controller has two inputs (e and Δe) and only one output (see Figure A2). The fuzzy rules of the designed modulation technology are given in Table A2. 49 rules (7 × 7) were selected to have the most robust fuzzy controller and good results for the generated current. The purpose of using K1, K2, and K3 is to adjust the fuzzy logic controller and improve the results obtained, as well as the value of THD for the electric current and was determined by the trial-and-error technique.

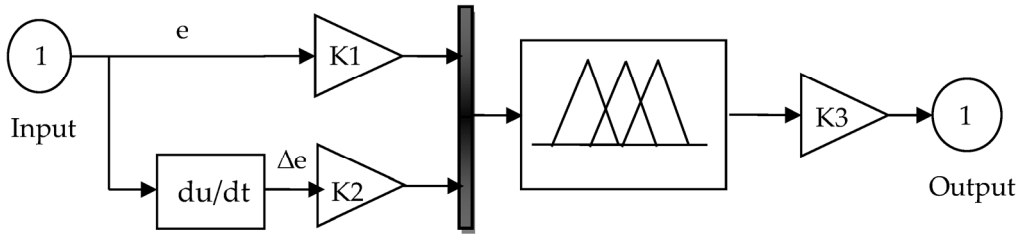

Figure A2. Structure of the FLC.

Table A2. Fuzzy rules of the hysteresis comparators.

e / **Δe**	**NB**	**NM**	**NS**	**EZ**	**PS**	**PM**	**PB**
PB	EZ	PS	PM	PB	PB	PB	PB
EZ	NB	NM	NS	EZ	PS	PM	PB
NM	NB	NB	NB	NM	NS	EZ	PS
NB	NB	NB	NB	NB	NM	NS	EZ
PM	NS	EZ	PS	PM	PB	PB	PB
PS	NM	NS	EZ	PS	PM	PB	PB
NS	NB	NB	NM	NS	EZ	PS	PM

Referring to Table A2 the membership functions (MF) are the following: NL defines the negative large; NM and NS are the negative medium and the negative small, respectively. ZR is zero, while PL, PM, and PS are the positive large, positive medium, and the positive small, respectively. The rule base is the core part of the fuzzy logic controller, which is designed based on process dynamics, and the experience and knowledge of experts.

The MFs also play a vital role in the overall performance of fuzzy representation. MFs are the basic elements of fuzzy set theory, i.e., the fuzziness of a fuzzy set is determined by its MF. Accordingly, the shapes of MFs are important for a particular problem since they affect a fuzzy inference system. They may have different shapes such as triangular, trapezoidal, Gaussian, and so forth [55]. In this paper, triangular shapes have been used.

A fuzzy logic set in the universe X is characterized by an MF, $\mu_A(x)$, which takes values on the interval [0, 1] and can be represented as a set of ordered pairs of an element. In this paper, seven triangular MFs were chosen for the inputs of the fuzzy logic controller, which are shown in Figure A3. The maximum and minimum values of the universe of discourse for all inputs and output were −10 to +10.

In fuzzy control, there are usually used two types of Fuzzy Inference Systems (FIS): Mamdani and Sugeno. Fuzzification is the conversion of a precise quantity to a fuzzy quantity, instead, defuzzification is the conversion of a fuzzy quantity to a precise quantity. It has been proposed by investigators in recent years, among popular defuzzification methods: Bisector, Mean of Maximum, Centroid, Smallest of Maximum, and Largest of Maximum. However, the type of FIS used in this work is Mamdani and Centroid was also used for defuzzification. The selection Centroid of area defuzzification method is used because it has been used generally and gives more reliable results than the others. Furthermore, the center of area defuzzification method is suitable for a multidimensional fuzzy output. However, the selection of the defuzzification technique is critical and has a significant impact on the speed and accuracy of the fuzzy model.

On the other hand, several characteristics must be known and carefully chosen to form and create fuzzy logic, for example, implication, aggregation, defuzzification method, etc. The parameters of the proposed fuzzy controller are given in Table A3. Through this table, it is possible to know the fuzzy characteristics used in this work, such as FIS type, defuzzification, implication, and method, or method and aggregation.

After the inputs are fuzzified, an appropriate rule-base should be developed using the inputs and the outputs, which can be described as:

If (e is NG) and (Δe is NG) then (Y is NG)

If (e is NM) and (Δe is NP) then (Y is NG)

where e and Δe are the inputs of the fuzzy sets, and y is the output of the fuzzy sets.

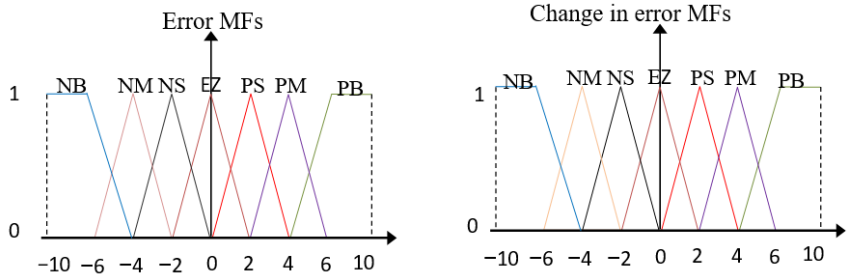

a) Error (e) **b)** Change in error (Δe)

Figure A3. Membership functions for inputs.

Table A3. Parameters of the fuzzy logic controller.

Or method	Max
And method	Min
FIS type	Mamdani
Defuzzification	Centroid
Implication	Min
Aggregation	Max

The surface, mesh, quiver, and rule of the fuzzy logic controller are illustrated in Figure A4, Figure A5, Figure A6, and Figure A7, respectively.

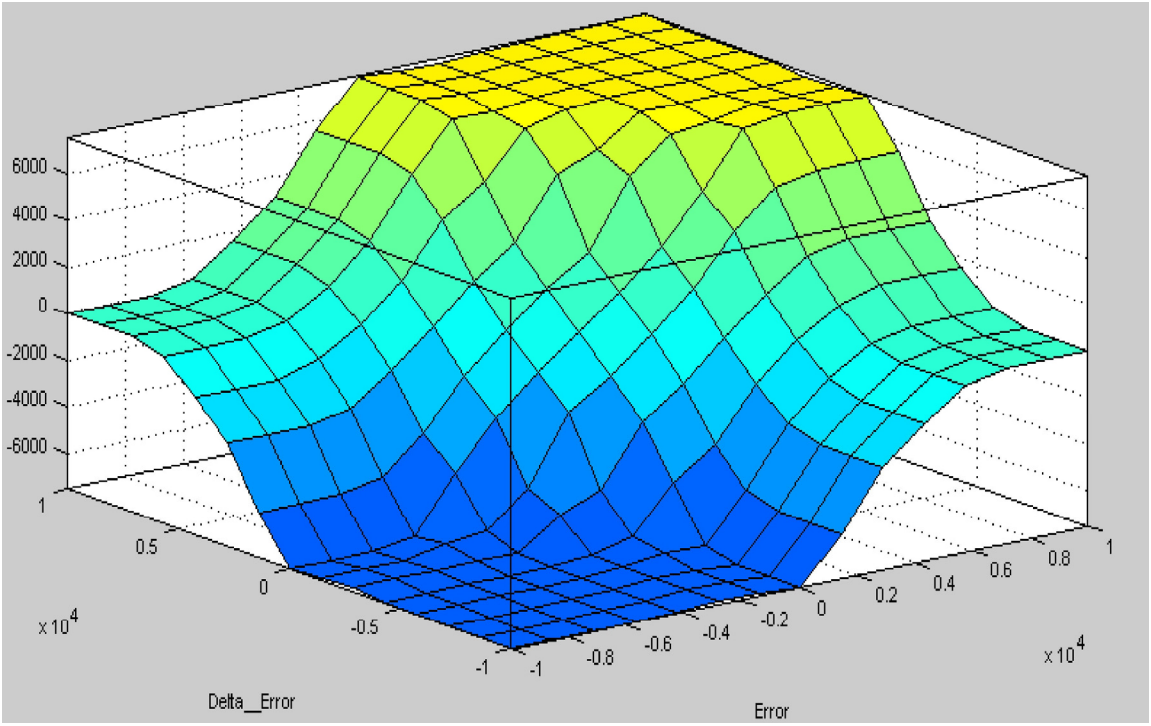

Figure A4. Surface.

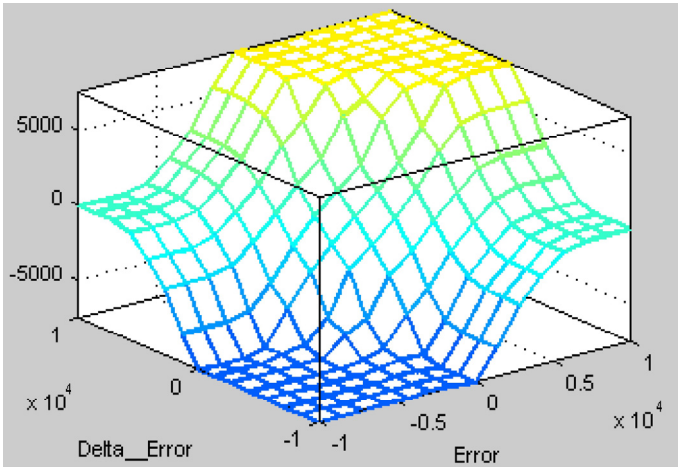

Figure A5. Mesh. The figure has been changed.

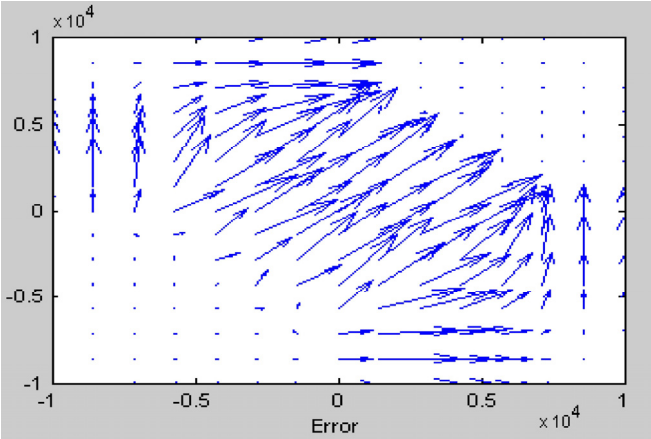

Figure A6. Quiver.

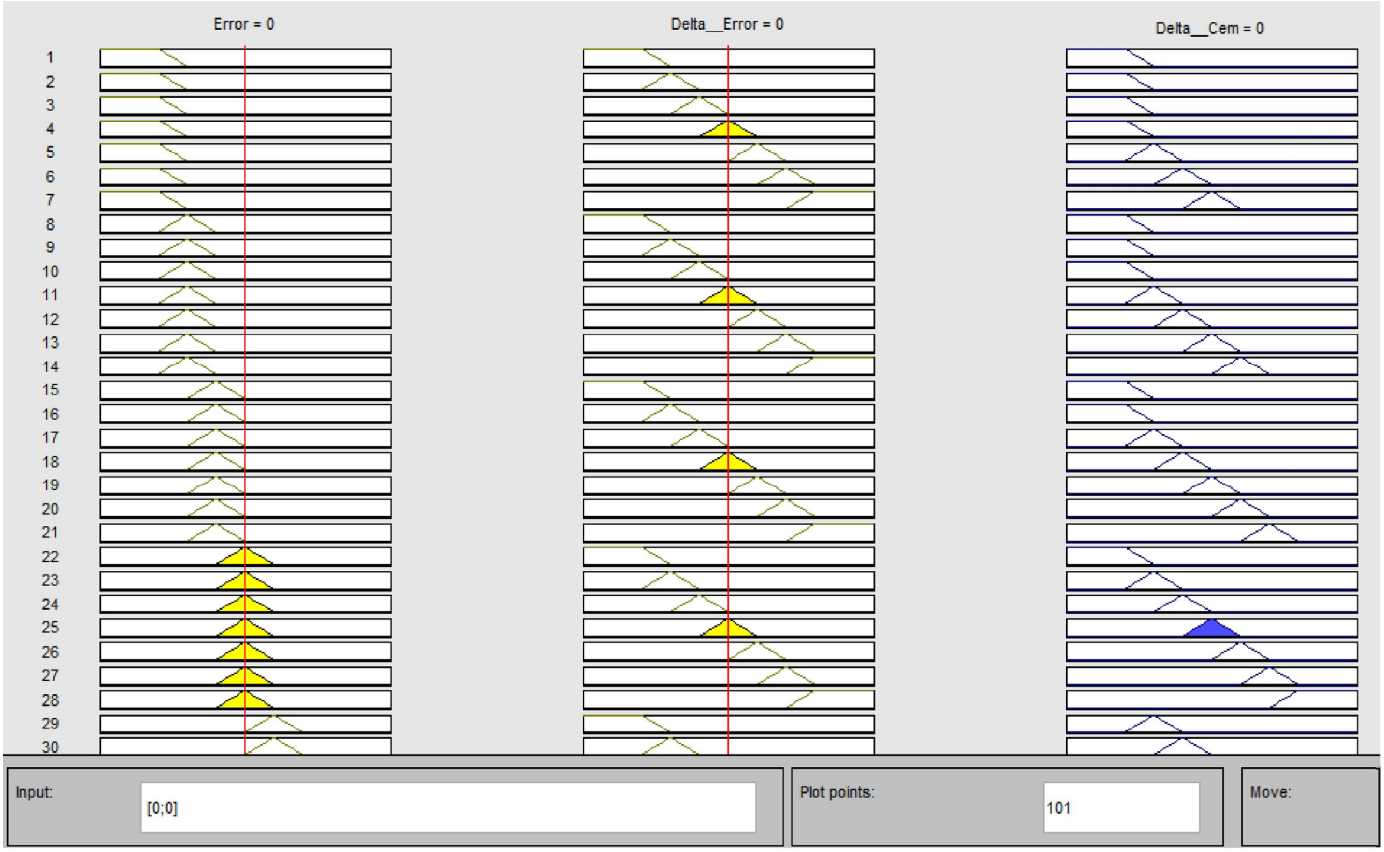

Figure A7. Rule.

Appendix C. Design of the Feedforward Neural Network

The design of the feedforward neural networks (FNNs) will be detailed here. This algorithm is similar to the conventional neural network. This algorithm does not need the mathematical model of systems [58]. However, FNNs are also multi-layered networks of neurons (MLN). This type of network is called feedforward because the information only travels forward in the neural network, through the input modes then through the hidden layers (single or many layers), and finally through the output modes. The FNN doesn't require a prior mathematical model. A learning algorithm is used during the training and learning phase to adjust sequentially by trial and error the synaptic weights of the neurons. In order to train the FNN controllers, we used the Levenberg-Marquardt backpropagation.

This method is a simple algorithm. However, the FNN controllers structure consists of 3 layers: output layer, hidden layer, and input layer. An example of the learning process in an FNN applied to the identification of PI controller is shown in Figure A8. In this context, the input vectors are the errors of the active and reactive powers, and the output vectors are the direct and quadrature rotor voltages.

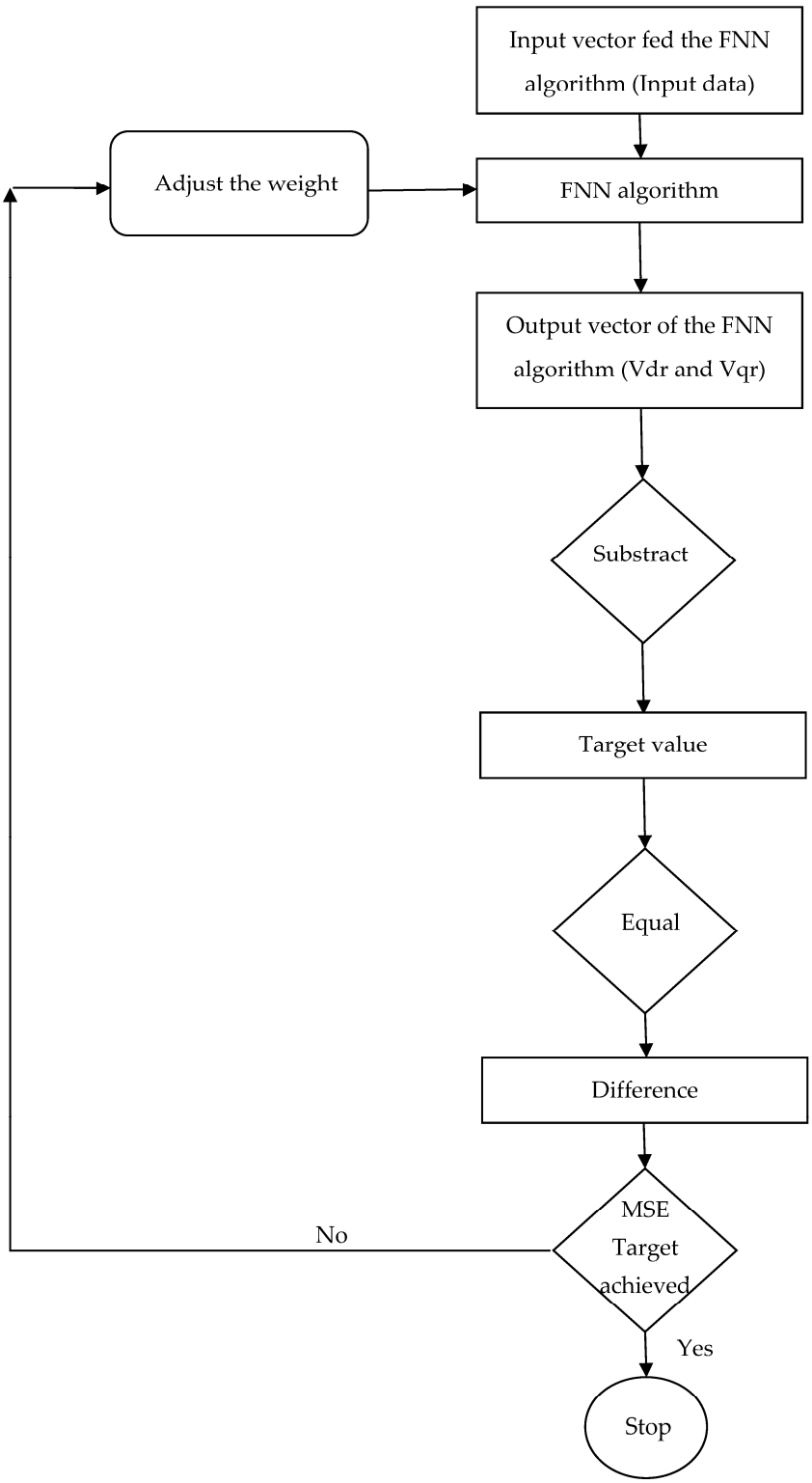

Figure A8. A learning algorithm in an FNN model.

There is no certain criterion in FNN control for selecting the number of neurons in the hidden layer, but enough neurons are needed to obtain the desired characteristic [59]. Generally, in designing and training the FNN, certain considerations have to be taken to be able to get the best result, i.e., by choosing the number and types of neurons in the hidden layer to find the best solution, avoiding local minima in the error space.

By Equation (A1), the value of the hidden layer can be easily calculated:

$$v_j = (1 + \exp\left(-1 + \sum_{i=1}^{1} x_i W_{ij}\right))^{-1}, \; j = 1, \ldots, \; J \tag{A1}$$

where v_j represents the jth neuron in the hidden layer, x_i represents the ith neuron in the input layer, and the weight between neurons is represented by W_{ij}.

The output layer node value can be computed using Equation (A2).

$$m = (1 + \exp\left(-1 + \sum_{j=1}^{j} v_j W_{ij}\right))^{-1} \tag{A2}$$

where m represents the output layer mode.

The error between actual and computed data has been calculated using Equation (A3):

$$E_{rr} = \frac{1}{2}(a - m)^2 \tag{A3}$$

where a represents the propagation form of the actual data for the output and the hidden layers, as expressed in Equations (A4) and (A5), respectively.

$$\delta_y = (a - m)(1 - m) \tag{A4}$$

$$\delta_m = v_j(a - v_j)(1 - y)\delta_m W_{j1}, \qquad j = 1, \ldots J \tag{A5}$$

The weight adjustment between layers can be carried out using Equations (A6) and (A7):

$$\Delta W_{ij} = \alpha \delta_m . v_j, \quad i = 1 \ldots I, \; j = 1 \ldots . J \tag{A6}$$

$$\Delta W_{ij}^n = \alpha \delta_m . v_j, \quad j = 1 \ldots . J \tag{A7}$$

where α represents the learning rate and, additionally, momentum can be measured as Equations (A8) and (A9), respectively.

$$\Delta W_{ij}^n = \alpha \delta_m . v_j + \beta \Delta W_{j1}^{n-1}, \quad j = 1 \ldots . J \tag{A8}$$

$$\Delta W_{ij}^n = \alpha \delta_m . v_j + \beta \Delta W_{j1}^n, \quad i = 1 \ldots I, \; j = 1 \ldots . J \tag{A9}$$

where β represents momentum constant and n indicates iterations of error backpropagation.

The training process in the flat region of the error surface avoids variations in the weights and has been accelerated using this momentum technique. Three types of functions can be used in the outer layer and the inner layer. These functions are the tang-sigmoid, linear, and logarithmic sigmoid functions.

The number of neurons in the hidden layer is obtained by trial-and-error exercises to have good results for both the effective power ripples and the THD value of the current.

To obtain an FNN controller, we need to designate several elements that represent one of the conditions for accomplishing this controller and they are explained in detail with the values taken in this work in Table A4.

Table A4. Parameters of the FNN controller.

Parameters	**Values**
Performances	Mean Squared Error (mse)
Training	Levenberg-Marquardt algorithm (trainlm)
TrainParam.show	50
TrainParam.Lr	0.05
Neurons of output layer	1
TrainParam.goal	0
TrainParam.mu	0.8
Neurons of input layer	1
Coeff. of acceleration of convergence (mc)	0.9
Derivative	Default (default deriv)
Number of hidden layers	1
Functions of activation	Tensing, Purling, trainlm
Number of output layer	1
TrainParam.eposh	250
Number of input layer	1
Neurons of hidden layer	8

In neural networks, output and input layer neurons are selected according to the number of inputs and outputs of the system, respectively. The number of entries is one in the entry layer, so the number of cells is only one. As for the output layer, there is only one output, so there is only one cell.

The neurons of the hidden layer are chosen randomly and there is no rule for choosing them. This is the real problem with neural networks that there is no rule for selecting both the neurons of the hidden layer and even the number of hidden layers.

In this work, we chose only one hidden layer and the neurons were randomly selected, and the choice that we got from it with a lower value for THD was used in this work, that is, we performed a series of experiments before choosing 8 neurons in the hidden layer. The structure diagram of the FNN for this paper is illustrated in Figure A9.

In an FNN method, the information moves only in the forward direction, from the input layer, through the hidden layers, and then to the output layer. There are no cycles or loops in this network. FNN methods are sometimes ambiguously called multilayer perceptron. This method can be expressed by the following equations:

$$Z = W^T \cdot x + b \tag{A10}$$

$$y = g(Z) \tag{A11}$$

$$y = g(\sum_{i=1}^{n} x_i \cdot W_i + b) \tag{A12}$$

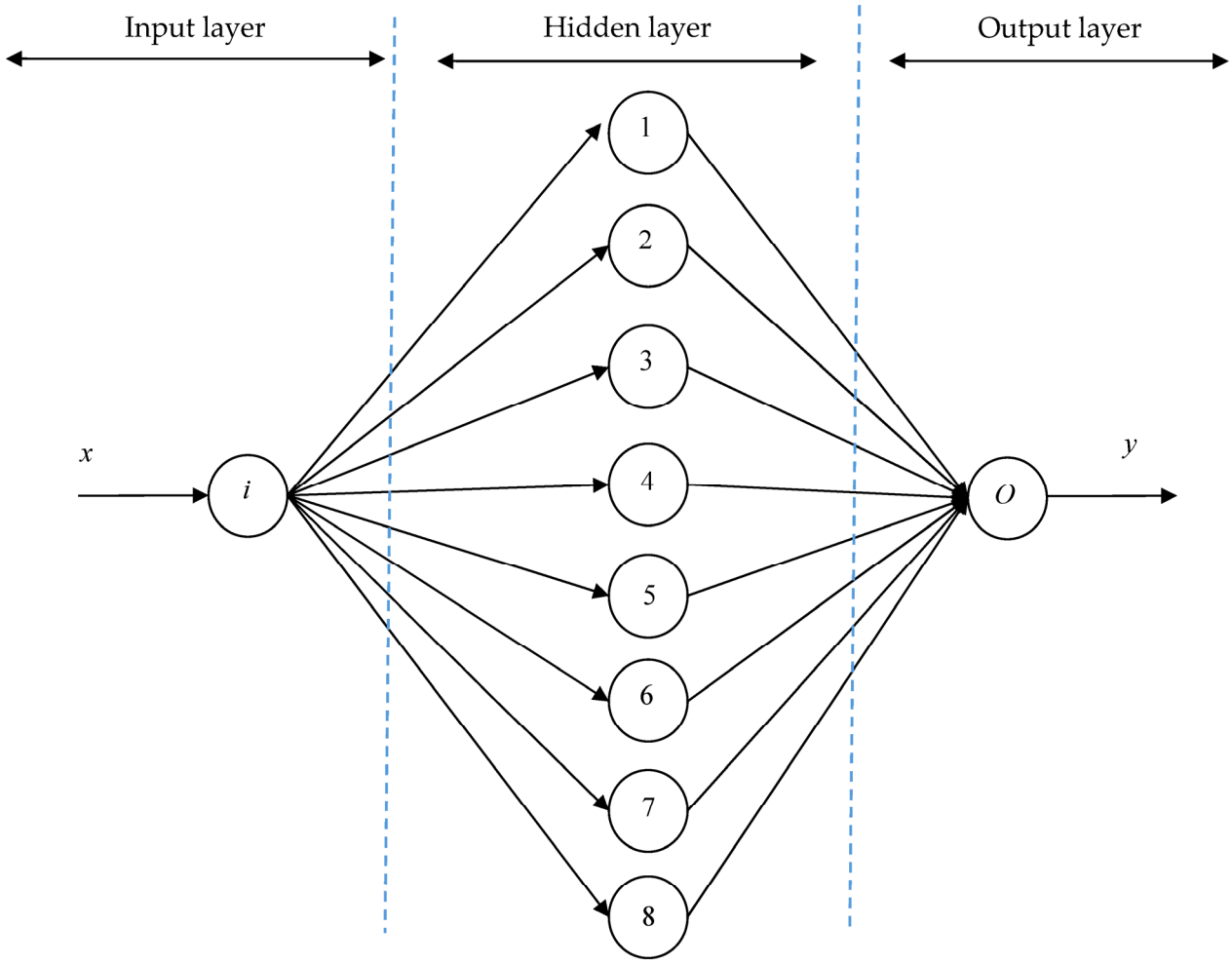

Figure A9. Structure diagram of the FNN in our designed learning-to-command model.

The activation function is chosen by the designer, but *Wi* and *b* are adjusted by some learning rules during the training process of the neural network.

$$y = g(Z) = \begin{cases} 0 & if\ Z \leq 0 \\ 1 & if\ Z > 0 \end{cases} \tag{A13}$$

In this work, the weight and bias of the neural network are selected based on the use of a Levenberg-Marquardt algorithm (LMA). This is by using the word *trainlm* in the Matlab software. However, the LMA technique is a robust algorithm and quick technique compared to other methods. The neural network training is shown in Figure A10. Figure A11 shows the training plot of the FNN controller. From this figure, the best training performance is 8.8189 at epoch 250. The error plot of the FNN algorithm is shown in Figure A12. Through this picture, we find that the targeting field is [−30, 30] and the training value is R = 0.51025, and the output is given by (output = 0.26*Target+8.6). On the other hand, Gradient, Mu, and Validation Checks are shown in Figure A13 and they represent the properties of the FNN algorithm. From this figure, the best Gradient, Mu, and validation checks are 0.021851, 9000, and 0 at epoch 250, respectively.

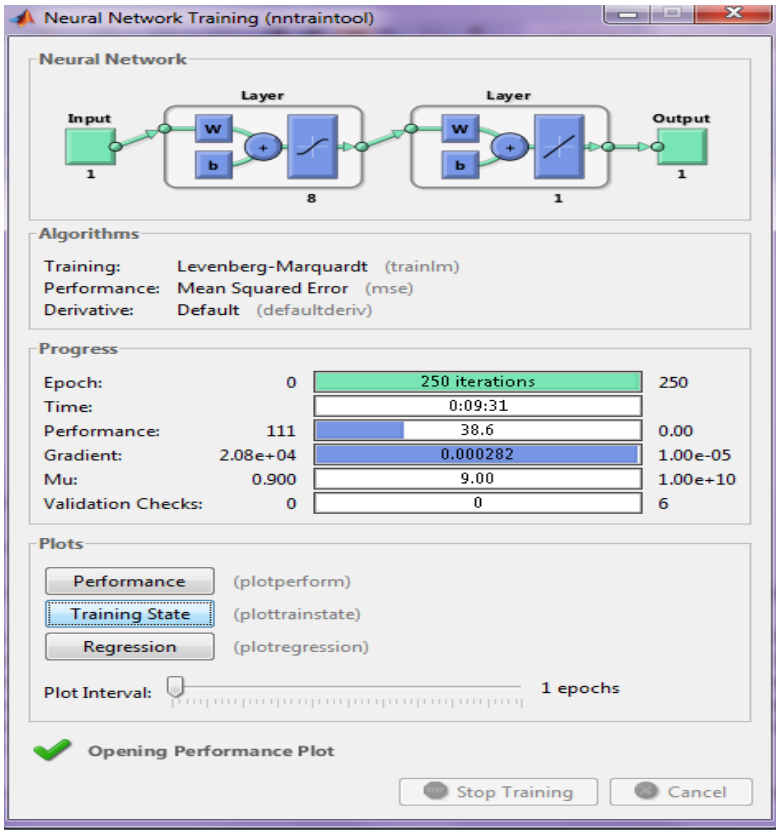

Figure A10. Neural network training.

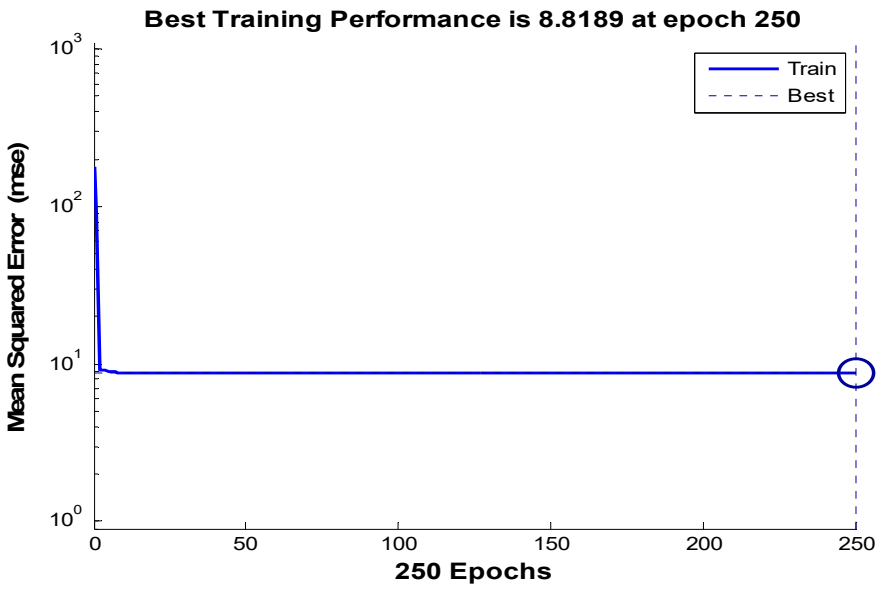

Figure A11. Training plot.

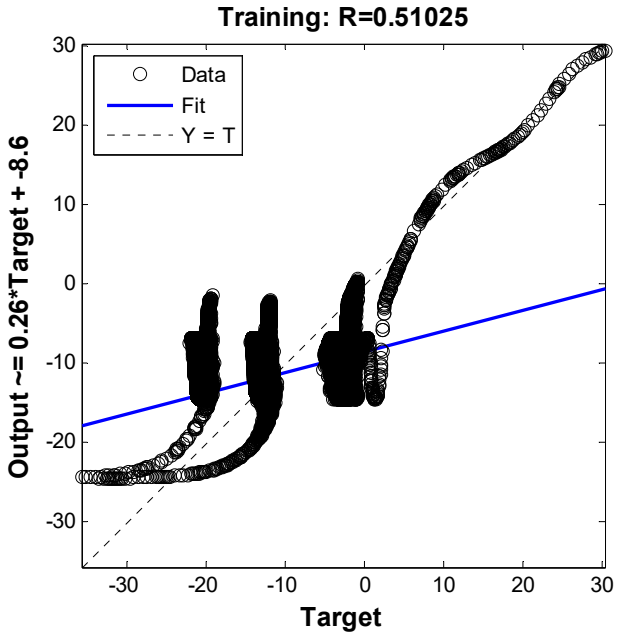

Figure A12. Error plot.

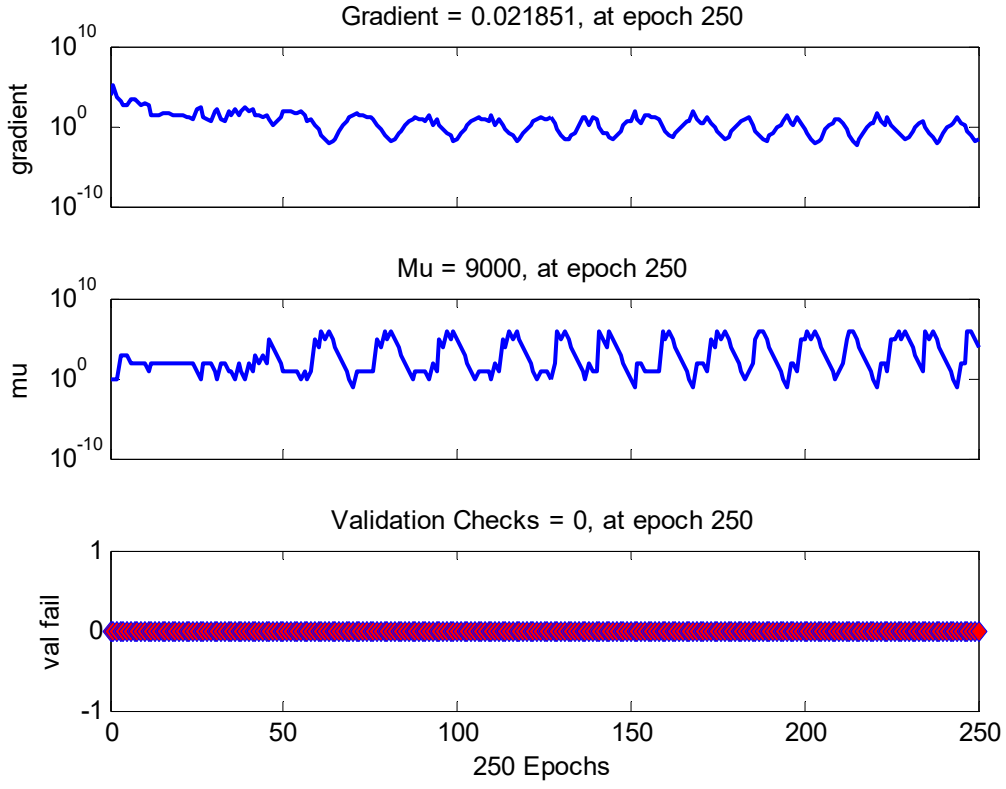

Figure A13. Characteristics of the FNN controller.

References

1. Kumar, P.M.; Sivalingam, K.; Lim, T.-C.; Ramakrishna, S.; Wei, H. Strategies for Enhancing the Low Wind Speed Performance of H-Darrieus Wind Turbine—Part 1. *Clean Technol.* **2019**, *1*, 185–204. [CrossRef]
2. Kumar, P.M.; Sivalingam, K.; Lim, T.-C.; Ramakrishna, S.; Wei, H. Review on the Evolution of Darrieus Vertical Axis Wind Turbine: Large Wind Turbines. *Clean Technol.* **2019**, *1*, 205–223. [CrossRef]

3. Manousakis, N.; Psomopoulos, C.; Ioannidis, G.; Kaminaris, S. A Binary Integer Programming Method for Optimal Wind Turbines Allocation. *Clean Technol.* **2021**, *3*, 462–473. [CrossRef]
4. AlGhamdi, S.; Hamdan, I.; Youssef, M.; Noureldeen, O. Development and Application of Fuzzy Proportional-Integral Control Scheme in Pitch Angle Compensation Loop for Wind Turbines. *Machines* **2021**, *9*, 135. [CrossRef]
5. Abdelrahem, M.; Hackl, C.; Kennel, R. Limited-Position Set Model-Reference Adaptive Observer for Control of DFIGs without Mechanical Sensors. *Machines* **2020**, *8*, 72. [CrossRef]
6. Chen, H.; Xie, W.; Chen, X.; Han, J.; Aït-Ahmed, N.; Zhou, Z.; Tang, T.; Benbouzid, M. Fractional-Order PI Control of DFIG-Based Tidal Stream Turbine. *J. Mar. Sci. Eng.* **2020**, *8*, 309. [CrossRef]
7. Alhato, M.; Ibrahim, M.; Rezk, H.; Bouallègue, S. An Enhanced DC-Link Voltage Response for Wind-Driven Doubly Fed Induction Generator Using Adaptive Fuzzy Extended State Observer and Sliding Mode Control. *Mathematics* **2021**, *9*, 963. [CrossRef]
8. Cortajarena, J.A.; Barambones, O.; Alkorta, P.; Cortajarena, J. Grid Frequency and Amplitude Control Using DFIG Wind Turbines in a Smart Grid. *Mathematics* **2021**, *9*, 143. [CrossRef]
9. Alhato, M.M.; Bouallègue, S.; Rezk, H. Modeling and Performance Improvement of Direct Power Control of Doubly-Fed Induction Generator Based Wind Turbine through Second-Order Sliding Mode Control Approach. *Mathematics* **2020**, *8*, 2012. [CrossRef]
10. Giaourakis, D.G.; Safacas, A.N. Effect of Short-Circuit Faults in the Back-to-Back Power Electronic Converter and Rotor Terminals on the Operational Behavior of the Doubly-Fed Induction Generator Wind Energy Conversion System. *Machines* **2015**, *3*, 2–26. [CrossRef]
11. Benbouhenni, H.; Lemdani, S. Combining synergetic control and super twisting algorithm to reduce the active power undulations of doubly fed induction generator for dual-rotor wind turbine system. *Electr. Eng. Electromechanics* **2021**, 8–17. [CrossRef]
12. Zahedi, A.H.; Arab, M.G.; Taghipour, B.S. Sliding Mode and Terminal Sliding Mode Control of Cascaded Doubly Fed In-duction Generator. *IJEEE* **2021**, *17*, 1955. Available online: http://ijeee.iust.ac.ir/article-1-1955-en.html (accessed on 1 September 2021).
13. Hosseinabadi, M.; Rastegar, H. DFIG Based Wind Turbines Behavior Improvement during Wind Variations using Fractional Order Control Systems. *IJEEE* **2014**, *10*, 314–323. Available online: http://ijeee.iust.ac.ir/article-1-663-en.html (accessed on 1 September 2021).
14. Pour Ebrahim, R.; Tohidi, S.; Younesi, A. Sensorless Model Reference Adaptive Control of DFIG by Using High Frequency Signal Injection and Fuzzy Logic Control. *IJEEE* **2018**, *14*, 11–21. [CrossRef]
15. Heydari, E.; Rafiee, M.; Pichan, M. Fuzzy-Genetic Algorithm-Based Direct Power Control Strategy for DFIG. *IJEEE* **2018**, *14*, 353–361. Available online: http://ijeee.iust.ac.ir/article-1-1185-en.html (accessed on 1 September 2021).
16. Djeriri, Y. Lyapunov-Based Robust Power Controllers for a Doubly Fed Induction Generator. *IJEEE* **2020**, *16*, 551–558. Available online: http://ijeee.iust.ac.ir/article-1-1596-en.html (accessed on 1 September 2021).
17. Kaloi, G.S.; Baloch, M.H.; Kumar, M.; Soomro, D.M.; Chauhdary, S.T.; Memon, A.A.; Ishak, D. An LVRT Scheme for Grid Connected DFIG Based WECS Using State Feedback Linearization Control Technique. *Electronics* **2019**, *8*, 777. [CrossRef]
18. Mossa, M.A.; Echeikh, H.; Diab, A.A.Z.; Quynh, N.V. Effective Direct Power Control for a Sensor-Less Doubly Fed Induction Generator with a Losses Minimization Criterion. *Electronics* **2020**, *9*, 1269. [CrossRef]
19. Peng, X.; Chen, R.; Zhou, J.; Qin, S.; Bi, R.; Sun, H. Research on Mechanism and Damping Control Strategy of DFIG-Based Wind Farm Grid-Connected System SSR Based on the Complex Torque Method. *Electronics* **2021**, *10*, 1640. [CrossRef]
20. Cui, H.; Li, X.; Wu, G.; Song, Y.; Liu, X.; Luo, D. MPC Based Coordinated Active and Reactive Power Control Strategy of DFIG Wind Farm with Distributed ESSs. *Energies* **2021**, *14*, 3906. [CrossRef]
21. Han, Y.; Ma, R. Adaptive-Gain Second-Order Sliding Mode Direct Power Control for Wind-Turbine-Driven DFIG under Balanced and Unbalanced Grid Voltage. *Energies* **2019**, *12*, 3886. [CrossRef]
22. Medeiros, A.; Ramos, T.; De Oliveira, J.T.; Júnior, M.F.M. Direct Voltage Control of a Doubly Fed Induction Generator by Means of Optimal Strategy. *Energies* **2020**, *13*, 770. [CrossRef]
23. Sami, I.; Ullah, S.; Ali, Z.; Ullah, N.; Ro, J.-S. A Super Twisting Fractional Order Terminal Sliding Mode Control for DFIG-Based Wind Energy Conversion System. *Energies* **2020**, *13*, 2158. [CrossRef]
24. Han, Y.; Li, S.; Du, C. Adaptive Higher-Order Sliding Mode Control of Series-Compensated DFIG-Based Wind Farm for Sub-Synchronous Control Interaction Mitigation. *Energies* **2020**, *13*, 5421. [CrossRef]
25. Cheng, P.; Wu, C.; Ning, F.; He, J. Voltage Modulated DPC Strategy of DFIG Using Extended Power Theory under Unbalanced Grid Voltage Conditions. *Energies* **2020**, *13*, 6077. [CrossRef]
26. Ma, R.; Han, Y.; Pan, W. Variable-Gain Super-Twisting Sliding Mode Damping Control of Series-Compensated DFIG-Based Wind Power System for SSCI Mitigation. *Energies* **2021**, *14*, 382. [CrossRef]
27. Brando, G.; Dannier, A.; Spina, I. Performance Analysis of a Full Order Sensorless Control Adaptive Observer for Doubly-Fed Induction Generator in Grid Connected Operation. *Energies* **2021**, *14*, 1254. [CrossRef]
28. Kroplewski, P.; Morawiec, M.; Jąderko, A.; Odeh, C. Simulation Studies of Control Systems for Doubly Fed Induction Generator Supplied by the Current Source Converter. *Energies* **2021**, *14*, 1511. [CrossRef]
29. Napole, C.; Barambones, O.; Derbeli, M.; Cortajarena, J.; Calvo, I.; Alkorta, P.; Bustamante, P. Double Fed Induction Generator Control Design Based on a Fuzzy Logic Controller for an Oscillating Water Column System. *Energies* **2021**, *14*, 3499. [CrossRef]
30. Susperregui, A.; Herrero, J.M.; Martinez, M.I.; Tapia-Otaegui, G.; Blasco, X. Multi-Objective Optimisation-Based Tuning of Two Second-Order Sliding-Mode Controller Variants for DFIGs Connected to Non-Ideal Grid Voltage. *Energies* **2019**, *12*, 3782. [CrossRef]

31. Mondal, S.; Kastha, D. Improved Direct Torque and Reactive Power Control of a Matrix-Converter-Fed Grid-Connected Doubly Fed Induction Generator. *IEEE Trans. Ind. Electron.* **2015**, *62*, 7590–7598. [CrossRef]
32. Hu, J.; Nian, H.; Hu, B.; He, Y.; Zhu, Z.Q. Direct Active and Reactive Power Regulation of DFIG Using Sliding-Mode Control Approach. *IEEE Trans. Energy Convers.* **2010**, *25*, 1028–1039. [CrossRef]
33. Martinez, M.I.; Tapia, G.; Susperregui, A.; Camblong, H. Sliding-Mode Control for DFIG Rotor- and Grid-Side Converters Under Unbalanced and Harmonically Distorted Grid Voltage. *IEEE Trans. Energy Convers.* **2012**, *27*, 328–339. [CrossRef]
34. Ullah, N.; Sami, I.; Chowdhury, S.; Techato, K.; Alkhammash, H.I. Artificial Intelligence Integrated Fractional Order Control of Doubly Fed Induction Generator-Based Wind Energy System. *IEEE Access* **2020**, *9*, 5734–5748. [CrossRef]
35. De Marchi, R.A.; Dainez, P.S.; Von Zuben, F.J.; Bim, E. A Multilayer Perceptron Controller Applied to the Direct Power Control of a Doubly Fed Induction Generator. *IEEE Trans. Sustain. Energy* **2014**, *5*, 498–506. [CrossRef]
36. Erazo-Damian, I.; Apsley, J.M.; Perini, R.; Iacchetti, M.F.; Marques, G.D. Stand-Alone DFIG FOC Sensitivity and Stability Under Mismatched Inductances. *IEEE Trans. Energy Convers.* **2018**, *34*, 860–869. [CrossRef]
37. Iacchetti, M.F.; Marques, G.; Perini, R. Torque Ripple Reduction in a DFIG-DC System by Resonant Current Controllers. *IEEE Trans. Power Electron.* **2014**, *30*, 4244–4254. [CrossRef]
38. Marques, G.D.; Iacchetti, M.F. DFIG Topologies for DC Networks: A Review on Control and Design Features. *IEEE Trans. Power Electron.* **2018**, *34*, 1299–1316. [CrossRef]
39. Prasad, R.M.; Mulla, M.A. A Novel Position-Sensorless Algorithm for Field-Oriented Control of DFIG With Reduced Current Sensors. *IEEE Trans. Sustain. Energy* **2018**, *10*, 1098–1108. [CrossRef]
40. Prasad, R.M.; Mulla, M.A. Mathematical Modeling and Position-Sensorless Algorithm for Stator-Side Field-Oriented Control of Rotor-Tied DFIG in Rotor Flux Reference Frame. *IEEE Trans. Energy Convers.* **2019**, *35*, 631–639. [CrossRef]
41. Benbouhenni, H. Comparative Study between direct vector control and fuzzy sliding mode controller in three-level space vector modulation inverter of reactive and active power command of DFIG-based wind turbine systems. *Int. J. Smart Grid* **2018**, *2*, 188–196.
42. Benbouhenni, H. Neuro-second order sliding mode field oriented control for DFIG based wind turbine. *Int. J. Smart Grid* **2018**, *2*, 209–217.
43. Habib, B.; Boudjema, Z.; Belaidi, A. Direct vector control of a DFIG supplied by an intelligent SVM inverter for wind turbine system. *Iran. J. Electr. Electron. Eng.* **2019**, *15*, 45–55.
44. Habib, B.; Boudjema, Z.; Belaidi, A. Indirect vector control of a DFIG supplied by a two-level FSVM inverter for wind turbine system. *Majlesi J. Electron. Eng.* **2019**, *13*, 45–54.
45. Amrane, F.; Chaiba, A. A novel direct power control for grid-connected doubly fed induction generator based on hybrid arti-ficial intelligent control with space vector modulation. *Rev. Sci. Tech. Electrotechnol. Energy* **2016**, *61*, 263–268.
46. Amrane, F.; Chaiba, A.; Babas, B.E.; Mekhilef, S. Design and implementation of high performance field oriented control for grid-connected doubly fed induction generator via hysteresis rotor current controller. *Rev. Sci. Tech. Electrotechn. Energy* **2016**, *61*, 319–324.
47. Boulaam, K.; Mekhilef, A. Output power control of a variable wind energy conversion system. *Rev. Sci. Tech. Electrotechnol. Energy* **2017**, *62*, 197–202.
48. Kazmierkowski, M.P.; Malesani, L. Current control techniques for three-phase voltage-source PWM converters: A survey. *IEEE Trans. Ind. Electron.* **1998**, *45*, 691–703. [CrossRef]
49. Nnem, N.L.; Lonla, M.B.; Sonfack, G.B.; Mbih, J. Review of a Multipurpose Duty-Cycle Modulation Technology in Electrical and Electronics Engineering. *J. Electr. Eng. Electron. Control Comput. Sci.* **2021**, *4*, 9–18. Available online: https://jeeeccs.net/index.php/journal/article/view/101 (accessed on 1 September 2021).
50. El-Masry, E.I.; Yang, H.K.; Yakout, M.A. Implementations of artificial neural networks using current-mode pulse width modulation technique. *IEEE Trans. Neural Netw.* **1997**, *8*, 532–548. [CrossRef]
51. Tzou, Y.-Y.; Lin, S.-Y. Fuzzy-tuning current-vector control of a three-phase PWM inverter for high-performance AC drives. *IEEE Trans. Ind. Electron.* **1998**, *45*, 782–791. [CrossRef]
52. Zadeh, L. Fuzzy sets. *Inf. Control.* **1965**, *8*, 338–353. [CrossRef]
53. Tan, K.-H. Squirrel Cage Induction Generator System Using Wavelet Petri Fuzzy Neural Network Control for Wind Power Applications. *IEEE Trans. Power Electron.* **2015**, *31*, 1. [CrossRef]
54. Mas'Ud, A.A.; Ardila-Rey, J.A.; Albarracín, R.; Muhammad-Sukki, F.; Bani, N.A. Comparison of the Performance of Artificial Neural Networks and Fuzzy Logic for Recognizing Different Partial Discharge Sources. *Energies* **2017**, *10*, 1060. [CrossRef]
55. Ayrir, W.; Ourahou, M.; El Hassouni, B.; Haddi, A. Direct torque control improvement of a variable speed DFIG based on a fuzzy inference system. *Math. Comput. Simul.* **2018**, *167*, 308–324. [CrossRef]
56. Yahdou, A.; Hemici, B.; Boudjema, Z. Sliding mode control of dual rotor wind turbine system. *Mediterr. J. Meas. Control* **2015**, *11*, 412–419.
57. Yahdou, A.; Djilali, A.B.; Boudjema, Z.; Mehedi, F. Improved Vector Control of a Counter-Rotating Wind Turbine System Using Adaptive Backstepping Sliding Mode. *J. Eur. Syst. Autom.* **2020**, *53*, 645–651. [CrossRef]
58. Nag, S.; Lee, K. Neural Network-Based Control for Hybrid PV and Ternary Pumped-Storage Hydro Plants. *Energies* **2021**, *14*, 4397. [CrossRef]

59. Fayaz, M.; Ullah, I.; Kim, D. An Optimized Fuzzy Logic Control Model Based on a Strategy for the Learning of Membership Functions in an Indoor Environment. *Electronics* **2019**, *8*, 132. [CrossRef]
60. Ibrahim, Y.; Semmah, A.; Patrice, W. Neuro-Second Order Sliding Mode Control of a DFIG based Wind Turbine System. *J. Electr. Electron. Eng.* **2020**, *13*, 63–68.
61. Boudjema, Z.; Taleb, R.; Djeriri, Y.; Yahdou, A. A novel direct torque control using second order continuous sliding mode of a doubly fed induction generator for a wind energy conversion system. *Turk. J. Electr. Eng. Comput. Sci.* **2017**, *25*, 965–975. [CrossRef]
62. Amrane, F.; Francois, B.; Chaiba, A. Experimental investigation of efficient and simple wind-turbine based on DFIG-direct power control using LCL-filter for stand-alone mode. *ISA Trans.* **2021**. [CrossRef]
63. Yusoff, N.A.M.; Razali, A.M.; Karim, K.A.; Sutikno, T.; Jidin, A. A Concept of Virtual-Flux Direct Power Control of Three-Phase AC-DC Converter. *Int. J. Power Electron. Drive Syst. (IJPEDS)* **2017**, *8*, 1776–1784. [CrossRef]
64. Boudjema, Z.; Meroufel, A.; Djerriri, Y.; Bounadja, E. Fuzzy sliding mode control of a doubly fed induction generator for energy conversion. *Carpathian J. Electron. Comput. Eng.* **2013**, *6*, 7–14.
65. Yahdou, A.; Hemici, B.; Boudjema, Z. Second order sliding mode control of a dual-rotor wind turbine system by employing a matrix converter. *J. Electr. Eng.* **2016**, *16*, 1–11.
66. Yaichi, I.; Semmah, A.; Wira, P.; Djeriri, Y. Super-twisting Sliding Mode Control of a Doubly-fed Induction Generator Based on the SVM Strategy. *Period. Polytech. Electr. Eng. Comput. Sci.* **2019**, *63*, 178–190. [CrossRef]
67. Benbouhenni, H.; Bizon, N. A Synergetic Sliding Mode Controller Applied to Direct Field-Oriented Control of Induction Generator-Based Variable Speed Dual-Rotor Wind Turbines. *Energies* **2021**, *14*, 4437. [CrossRef]
68. Quan, Y.; Hang, L.; He, Y.; Zhang, Y. Multi-Resonant-Based Sliding Mode Control of DFIG-Based Wind System under Unbalanced and Harmonic Network Conditions. *Appl. Sci.* **2019**, *9*, 1124. [CrossRef]
69. Benbouhenni, H.; Bizon, N. Terminal Synergetic Control for Direct Active and Reactive Powers in Asynchronous Generator-Based Dual-Rotor Wind Power Systems. *Electronics* **2021**, *10*, 1880. [CrossRef]
70. El Ouanjli, N.; Derouich, A.; El Ghzizal, A.; Taoussi, M.; EL Mourabit, Y.; Mezioui, K.; Bossoufi, B. Direct torque control of doubly fed induction motor using three-level NPC inverter. *Prot. Control Mod. Power Syst.* **2019**, *4*, 1–9. [CrossRef]
71. Benbouhenni, H. Intelligent super twisting high order sliding mode controller of dual-rotor wind power systems with direct attack based on doubly-fed induction generators. *J. Electr. Eng. Electron. Control Comput. Sci.* **2021**, *7*, 1–8. Available online: https://jeeeccs.net/index.php/journal/article/view/219 (accessed on 1 September 2021).
72. Benbouhenni, H. Synergetic control theory scheme for asynchronous generator based dual-rotor wind power. *J. Electr. Eng. Electron. Control Comput. Sci.* **2021**, *7*, 19–28. Available online: https://jeeeccs.net/index.php/journal/article/view/215 (accessed on 1 September 2021).